



## Mid-to Late Holocene East Antarctic ice-core tephrochronology: Implications for reconstructing volcanic eruptions and assessing their climatic impacts over the last 5,500 years

Peter M. Abbott<sup>a,\*</sup>, Joseph R. McConnell<sup>b</sup>, Nathan J. Chellman<sup>b</sup>, Sepp Kipfstuhl<sup>c</sup>, Maria Hörl<sup>c</sup>, Johannes Freitag<sup>c</sup>, Eliza Cook<sup>d</sup>, William Hutchison<sup>e</sup>, Michael Sigl<sup>a</sup>

<sup>a</sup> Climate and Environmental Physics, Physics Institute, and Oeschger Centre for Climate Change Research, University of Bern, 3012, Bern, Switzerland

<sup>b</sup> Desert Research Institute, Nevada System of Higher Education, Reno, NV, 89512, USA

<sup>c</sup> Alfred Wegener Institute Helmholtz Centre for Polar and Marine Research, 27570, Bremerhaven, Germany

<sup>d</sup> Physics of Ice, Climate and Earth, Niels Bohr Institute, University of Copenhagen, 2200, Denmark

<sup>e</sup> School of Earth and Environmental Sciences, University of St. Andrews, St Andrews, KY16 9TS, UK



### ARTICLE INFO

Handling editor: Giovanni Zanchetta

**Keywords:**

Ice cores  
Antarctica  
Tephrochronology  
Cryptotephra  
Volcanic sulphur injections

### ABSTRACT

Ice cores are powerful archives for reconstructing volcanism as they contain both soluble (i.e. aerosols) and insoluble (i.e. tephra) products of volcanic eruptions and for more recent periods have high-precision annually resolved chronologies. The identification and geochemical analysis of cryptotephra in these cores can provide their volcanic source and latitude of injection, complementing records of sulphur injections from volcanic eruptions developed using continuous flow ice-core analysis. Here, we aim to improve the volcanic record for the Southern Hemisphere using a sampling strategy for cryptotephra identification based on coeval deposition of sulphate and microparticles in ice cores from the interior of East Antarctica covering the Mid-to Late Holocene. In total, 15 cryptotephras and one visible horizon were identified and geochemically characterised. Through comparisons to proximal deposits a range of possible sources were isolated for these horizons including the South Sandwich Islands, South Shetland Islands, Victoria Land (Antarctica) and South America. This new tephra framework contributes to the volcanic history of the region by extending the known geographical range of tephra deposition for previously identified events and providing a potential indication of phases of eruptive activity from key sources. Using the tephra-based source attributions and comparison of the timing of the events to a database of sulphur injections from Holocene volcanic eruptions it is possible to refine injection latitudes for some events, which can lead to improved estimates of their radiative forcing potential. The relatively low magnitude of the volcanic stratospheric sulphur injections related to the events in the tephra framework indicates they would have had a limited impact on Southern Hemisphere climate. Further work is required to improve source attributions for some events and/or to determine the magnitude of sulphur injections for individual events during years when coeval eruptions occurred. One limitation of the framework is the dominance of cryptotephra from regional volcanic sources and a lack of tephra from tropical sources, which hampers the refinement of eruption parameters for these large magnitude and often climate-impacting eruptions. This issue could be explored further through increased sampling of these events and/or development of additional analytical techniques for the identification and robust geochemical analysis of glass tephra shards less than 5 µm in diameter. Such investigations could be coupled with model experiments to determine the likelihood that past tropical eruptions deposited glass tephra shards over Antarctica and the potential size range and geographical spread of deposition.

\* Corresponding author.

E-mail address: [peter.abbott@unibe.ch](mailto:peter.abbott@unibe.ch) (P.M. Abbott).

## 1. Introduction

### 1.1. Reconstructing volcanism using ice-core records

Ice cores from both Greenland and Antarctica are powerful archives for reconstructing volcanism as they can preserve both soluble, i.e. aerosols, and non-soluble, i.e. tephra, products of volcanic eruptions from both local and distal volcanic sources (Abbott and Davies, 2012; Sigl et al., 2015, 2022; Narcisi and Petit, 2021). In addition, high-precision annually resolved chronologies have been developed for these records, particularly over Holocene timescales, which permit the accurate assignment of ages to eruptions (e.g. Sigl et al., 2015, 2022). The identification of tephra in ice cores in direct association with chemical indicators of volcanism, such as sulphate and conductivity, can significantly enhance volcanic reconstructions as geochemical characterisation of individual tephra shards allows an eruptive source to be isolated (Abbott and Davies, 2012). Such source attributions can add great value to the interpretation of ice-core records of volcanism, by contributing towards volcanic reconstructions, ascertaining the source and magnitude of aerosol emissions, evaluating the climatic impact of eruptions and assessing future volcanic risks (e.g. Pearce et al., 2004; Kurbatov et al., 2006; Bourne et al., 2016; Di Roberto et al., 2019; McConnell et al., 2020; Abbott et al., 2021b; Plunkett et al., 2022). Volcanic ash and acids also form isochrons that can constrain changes in ice-accumulation across Antarctica, which is key for providing a long-term context for projected ice loss and sea-level rise from continued global warming (e.g. Jacobel and Welch, 2005; DeConto and Pollard, 2016; Medley et al., 2018; Bodat et al., 2021, 2023; Stokes et al., 2022). However, while continuous records of chemical indicators of volcanism can be acquired relatively rapidly from ice cores using continuous melting systems (e.g. McConnell et al., 2002; Bigler et al., 2007; Severi et al., 2015) tephra records for specific cores are generally less developed due to the greater time required for direct ice sampling, identification and geochemical characterisation of tephra (Abbott and Davies, 2012). The difference in time required is particularly notable if the tephra horizons have no visible expression in the ice, i.e. cryptotephras (Davies, 2015), or do not directly relate to chemical signals in the ice (Abbott et al., 2012; Cook et al., 2022).

For the Antarctic region volcanic history can be reconstructed from proximal deposits or other palaeoclimatic archives, such as lacustrine sequences. Reconstructions, however, may be restricted by factors such as the relative inaccessibility and understudy of the volcanic regions, poor chronological control, sites dominantly recording local volcanism or data compilations focusing on a specific region (e.g. Baker, 1990; Björck et al., 1991b; Pearce et al., 1995; Haberle and Lumley, 1998;

Kraus et al., 2013; Del Carlo et al., 2018; Hopkins et al., 2021; Hopfenblatt et al., 2022a,b; Martínez Fontaine et al., 2023). Antarctic ice-core records of volcanism can complement these other archives as they can record volcanism from multiple local and distal sources, have a strong chronological framework and provide estimates of aerosol emissions.

### 1.2. Prior studies of tephra in Antarctic ice cores

Since the first reporting of tephra in Antarctic ice cores in the early 1980s (Kyle et al., 1981) many studies have aimed to identify tephra deposits in these records. Several of these have been conducted on shallow and deep ice cores from the interior of the East Antarctic Ice Sheet (EAIS) (e.g. EDML, EDC, Dome Fuji, South Pole, Vostok; Fig. 1), with many tephra horizons being identified (e.g. Palais et al., 1987, 1990, 1992; Fujii et al., 1999; Basile et al., 2001; Narcisi et al., 2005; Kohno et al., 2004, 2005; Narcisi and Petit, 2021). Beyond the Common Era, however, only one horizon, the so-called Vostok tephra dated to  $3.60 \pm 0.19$  ka BP on the AICC2012 timescale, has been identified in our study period (Narcisi and Petit, 2021; see Section 3.1.1). The low identification rate of Mid-to Late Holocene tephras in the interior of the EAIS is not attributed to a low incidence of volcanism or tephra deposition, but a focus on visible horizons in these records and the reconstruction of volcanism and synchronisation of records over their long time span of up to 800 kyr (Basile et al., 2001; Kohno et al., 2004; Narcisi et al., 2010b). These long-term studies provide an indication of the volcanic regions contributing tephra to the interior of the EAIS, with the majority of tephras sourced from the South Sandwich Islands, but it is also proposed that volcanic fallout can be correlated to volcanoes in the Antarctic Peninsula, West Antarctica and South America (Narcisi and Petit, 2021).

The East Antarctic TALDICE core contains a significant record of Mid-to Late Holocene tephra, including 12 visible and cryptotephra horizons reported in Narcisi et al. (2010a, 2012), with the cryptotephras identified based on anomalous grain size values. Retrieved from Talos Dome, adjacent to the Victoria Land mountains, the core site is proximal to the volcanoes of the McMurdo Volcanic Group (Fig. 1) and is a key recorder of local volcanism, such as eruptions of Mount Melbourne, alongside some eruptions thought to be from more distal volcanic regions, e.g. South America (Narcisi et al., 2012). One key horizon from a Northern Victoria Land volcano is the so-called Rittmann tephra ( $1252 \pm 2$  CE), sourced from Mount Rittmann, one of the volcanoes in the western Ross Sea area (Lee et al., 2019). Ice-core tephrochronological records of local volcanism also exist for volcanoes protruding through the West Antarctic Ice Sheet (WAIS), including Mount Takahe (e.g.

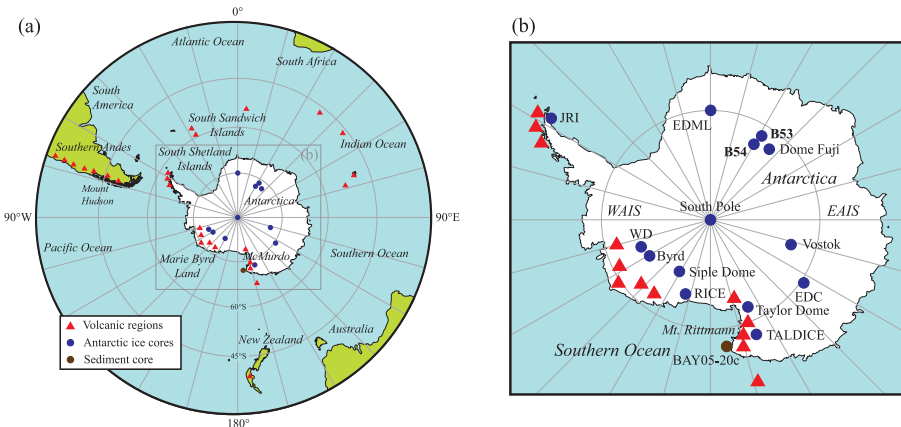


**Fig. 1.** (a) Map of Antarctica and the Southern Ocean region showing the location of Antarctic ice cores, volcanic regions that could have contributed tephra deposits to the records and specific volcanoes and sites mentioned in the text. (b) Inset focusing on Antarctica, the location of ice cores studied or mentioned in this work and local volcanic regions. WAIS = West Antarctic Ice Sheet; EAIS = East Antarctic Ice Sheet; JRI = James Ross Island; EDML = EPICA Dronning Maud Land; TALDICE = Talos Dome Ice Core; WD = West Antarctic Ice Sheet Divide Ice Core; EDC = EPICA Dome C; RICE = Roosevelt Island Climate Evolution Project ice core.

McConnell et al., 2017) and Mount Berlin in Marie Byrd Land. The Siple Dome ice core is a key archive for eruptions from these volcanoes, other local sources and potentially eruptions from South America, with several Mid-to Late Holocene eruptions identified (Dunbar et al., 2003; Kurbatov et al., 2006; Dunbar and Kurbatov, 2011). These tephra records are of interest as they provide evidence for East and West Antarctic volcanism during the Mid-to Late Holocene. To date, however, no deposits from these eruptions have been identified in cores from the interior of East Antarctica covering this time window, despite tephra from these sources being deposited over the region during earlier time periods (see Narcisi and Petit, 2021). This could be due to only local dispersal of the products of the eruptions or deposits are yet to be identified in these distal sites as they are only present as cryptotephras. Recent studies have highlighted the potential for widespread dispersal of small glass tephra shards and how cryptotephra identification can extend the known depositional envelopes for specific eruptions and volcanic centres (e.g. Lane et al., 2011; Jensen et al., 2014; Davies, 2015; Bourne et al., 2016).

While the studies highlighted above principally focused on multiple horizons in cores, several others have been conducted on specific Late Holocene eruptions thought to be sourced from low-latitude volcanoes with a global significance and/or a known historical age (e.g. Palais et al., 1990; Hartman et al., 2019; Narcisi et al., 2019). In these studies, chemical signals of volcanism were used to guide attempts to identify cryptotephra horizons. Palais et al. (1990) focused on volcanic events identified in the electrical conductivity record of an ice core from the South Pole. Fine glass shards were identified in several samples and following energy dispersive x-ray analysis they were linked to the known eruptions of Tambora, Indonesia 1815 CE, Huaynaputina, Peru 1600 CE and Nevado del Ruiz, Columbia 1595 CE and a then unknown eruption with sulphate peaking in 1259 CE. Subsequently compositionally similar glass from 1259 CE was found in a Greenland ice core (Palais et al., 1992), defining the only bipolar tephra horizon to date. The source was identified as Samalas, Indonesia (Lavigne et al., 2013) and the eruption was recently dated to Northern Hemisphere spring/summer of 1257 CE (Guillet et al., 2023) which is consistent with the cooling anomalies peaking in 1258 and 1259 CE (Büntgen et al., 2022). This 1259 CE volcanic event also was the focus of Narcisi et al. (2019) who analysed very fine glass tephra shards extracted from four East Antarctic ice cores and inferred they identified tephra from three roughly coeval eruptions: the Samalas eruption, an Antarctic, and a non-Antarctic eruption. Hartman et al. (2019) focused on a volcanic signal in the South Pole Ice Core (SPICEcore) dated to 1458 CE, which many studies have attributed to an eruption of the submarine Kuwae caldera, Vanuatu. Geochemical analyses of glass tephra shards preceding the rise of sulphate concentrations did not correlate to the products of Kuwae and the Reclus volcano, Chile, was suggested as the possible source (Hartman et al., 2019). However, Kuwae cannot be definitively ruled out as the source of the sulphate signal as this proposed source is inconsistent with the sulphur isotopic composition indicating a stratospheric sulphur source (Gautier et al., 2019; Burke et al., 2023). In addition, the overall ice-core chemical records during this period all feature the typical fingerprint (i.e. uniform, long-lasting deposition throughout Antarctica) left by large caldera-forming eruptions (e.g. Samalas 1257 CE, Tambora 1815 CE; Sigl et al., 2014). Aiming to test a disputed age for a recent eruption of the Taupō volcano, New Zealand, Piva et al. (2023) isolated rhyolitic tephra shards from this eruption in the Roosevelt Island Climate Evolution (RICE) ice core in ice with an age of  $230 \pm 19$  CE. Despite the large uncertainties for the ice-core age, due to volcanic synchronisation of this record to other Antarctic cores being challenging as there is significant marine sulphur deposition at the core site, it is consistent with the previously challenged radiocarbon wiggle-matched date of  $232 \pm 10$  CE and confirms its robustness.

### 1.3. Improving the Mid-to Late Holocene Antarctic tephra framework

Here we aim to improve the tephrochronological record for the

interior of East Antarctica for the Mid-to Late Holocene. We use a sampling strategy and identification method focused on identifying cryptotephras in two precisely dated ice-core sequences with highly resolved chemical records of volcanism. This represents the first intensive cryptotephra study for the interior of the East Antarctic Ice Sheet. Increasing the number of tephra-based source attributions for volcanic events recorded during this period has two purposes, firstly to improve the history of volcanism in the region and secondly to determine the magnitude of these eruptions relative to other Holocene eruptions and assess their potential climatic impact. There is also the potential to provide further insights into the dispersal of tephra from East and West Antarctic volcanoes known to be active during this period (see Section 1.2). Our focus on identifying cryptotephras in the records enhances the potential to source smaller magnitude or more distal eruptions that deposited low concentrations of tephra shards at the core locations.

## 2. Methods

For our tephrochronological investigations we have used two ice cores retrieved from a region in the interior of the East Antarctic Plateau that faces the Atlantic and Indian Ocean sectors of the Southern Ocean (Fig. 1). B53 ( $76.8^\circ\text{S}$ ,  $31.9^\circ\text{E}$ , 3737 m asl) and B54 ( $79^\circ\text{S}$ ,  $30^\circ\text{E}$ , 3473 m asl) were drilled in 2012/13 and 2016/17, respectively, by the Alfred Wegener Institute, Bremerhaven (Fig. 1). Sections from both cores have been measured at the Desert Research Institute, Reno, using a continuous melter system that incorporates two Element2 (Thermo Scientific) high-resolution inductively coupled plasma mass spectrometers operating in parallel to produce directly co-registered measurements of  $\sim 35$  elements, including sulphur, calcium and sodium (McConnell et al., 2002; Sigl et al., 2015; Maselli et al., 2017). In addition, co-registered measurements were made of the concentration of insoluble particles in the size ranges of  $2.5\text{--}5\ \mu\text{m}$  and  $5\text{--}10\ \mu\text{m}$  diameter using an inline Abakus® laser-based particle detector (Ruth et al., 2003). The data from B53 and B54 were synchronised to the seasonally resolved and annually counted WD2014 chronology (Sigl et al., 2016) using a series of volcanic markers as tie points to permit time-scale transfer.

A sampling strategy for tephra identification was devised based on sampling coeval peaks in the continuous records of fine insoluble particles and sulphur, corrected to non-sea-salt sulphur (nssS) concentrations to more closely reflect the volcanic signal (Sigl et al., 2013). The insoluble particle concentrations predominantly reflect dust deposition and therefore are not a direct proxy for the presence of tephra shards, but this measurement has been used successfully to identify cryptotephra horizons in both Greenland and Antarctic ice cores by targeting anomalous increases in insoluble particle concentrations (e.g. Jensen et al., 2014; Dunbar et al., 2017; McConnell et al., 2017, 2020; Plunkett et al., 2020, 2023; Smith et al., 2020; Abbott et al., 2021b). In total, we targeted 58 volcanic events between 3120 BCE and 1809 CE in B53 and 21 events in B54 between 2911 BCE and 1809 CE, with the B54 samples mainly focused on potentially tropical eruptions (Fig. 2). Based on chronological similarities, 16 of the sampled events can be regarded as common between the two cores. In addition, both cores contained a single visible tephra horizon that was sampled for geochemical analysis. For B53 the depth intervals covered by individual samples varied depending on the nature of the sulphur and particle peaks, e.g. width of peaks and the occurrence of double peaks, and the cross-sectional areas varied based on ice availability for sections of interest. The sample lengths varied between 3 and 26 cm, but were typically around 10 cm, and the cross-sectional areas ranged between  $1.7$  and  $15\ \text{cm}^2$ ; however most samples had a cross-section of  $\sim 9\ \text{cm}^2$ . For B54 the sample lengths were consistently 6 cm with a cross-sectional area of  $\sim 9\ \text{cm}^2$ .

Direct ice samples were prepared for tephra identification using optical microscopy and geochemical analysis using a protocol developed from methods for the analysis of ice-core and/or fine-grained glass tephra shards reported in several recent papers (e.g. Kuehn and Froese, 2010; Hall and Hayward, 2014; Iverson et al., 2017; Hartman et al.,

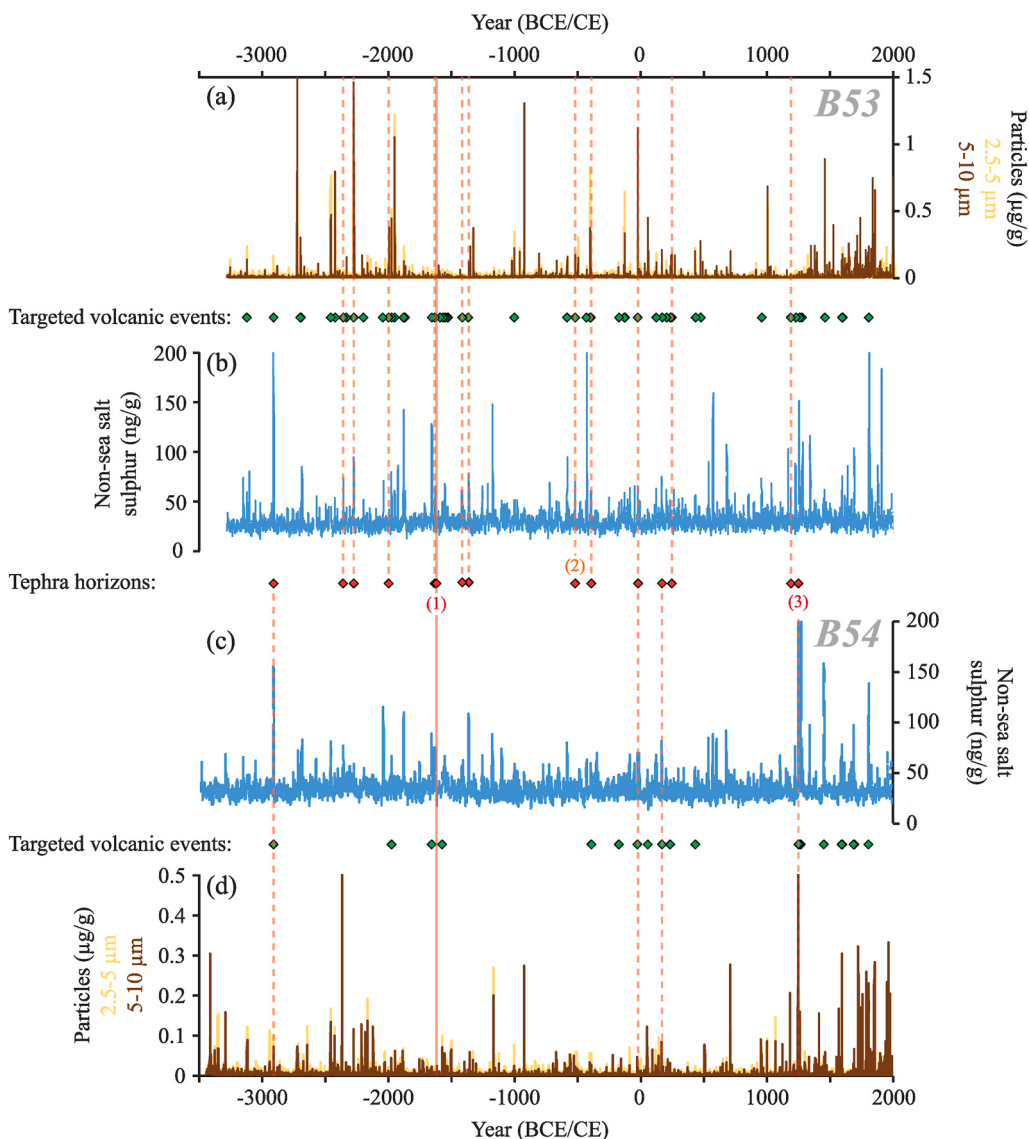


**Fig. 2.** Centimetre-resolution non-sea-salt-sulphur and insoluble particle (2.5–5  $\mu\text{m}$  and 5–10  $\mu\text{m}$  diameter) records from the (a and b) B53 and (c and d) B54 ice cores. The volcanic events targeted in the cores are denoted with green diamonds. Red diamonds denote samples containing geochemically characterised glass tephra shards and red dashed lines denote their position in the corresponding core. The solid red line represents a visible tephra horizon that can be correlated between the cores. Previously identified tephra horizons now isolated in B53 and/or B54 are labelled: (1) Vostok tephra (2) HW<sub>6</sub> (3) Rittmann tephra.

2019). Full details of our methodology are provided in the Supplementary Information. If glass tephra shards were present, they were analysed using wavelength dispersive (WDS) electron probe micro-analysis (EPMA) at the Institute of Geological Sciences, University of Bern. The concentrations of 10 major and minor elements in individual polished shards were analysed using a JEOL 8200 probe with five wavelength dispersive spectrometers, with the operating conditions of a 5  $\mu\text{m}$  beam diameter, a 2 nA beam current and an accelerating voltage of 15 kV. Pure metals, synthetic oxides and silicate samples were used for calibration (see Table S2). The secondary standards of Canneto Lami Lava, Lipari and BCR-2Ga were measured during the analytical periods to assess the precision and accuracy of the sample analyses and provide a cross-check between sessions (see Table S3). The sample analyses were initially filtered to remove analyses with total oxide values less than 90 wt%. Lower total oxide values for some analyses of fine-grained tephra shards could be due to the incorporation of resin in the interaction volume during analysis. This has been shown to have some impact on the precision of analyses but does not significantly affect the ratios between oxides (Iverson et al., 2017), however, using a 90 wt% total oxide

cut off will have removed analyses incorporating an excessive volume of resin. In addition, obviously erroneous analyses, such as those derived from the analysis of mineral particles or microlites within shards, were removed from the dataset. For further analysis and data comparisons, all data was normalised to an anhydrous basis (i.e. 100% total oxides). All the raw sample and secondary standard analyses are provided in the Supplementary Data (Tables S3–5). The number of analyses gained from each deposit is variable, from 1 to 28 individual analyses, but reflects the analytical challenges inherent to studies of ice-core tephra horizons, i.e. the small size and/or low concentration of glass shards present in these deposits.

Several samples, from which glass tephra shards were not identified based on optical microscopy, were selected for further analysis using backscatter electron (BSE) imaging and energy dispersive spectrometry (EDS), similar to the approach taken in Iverson et al. (2017). Samples were prioritised for this secondary check if their age relates to a notable volcanic event with an unknown source and/or a significant change in climate recorded in proxy archives. Analysis was carried out using a JEOL JXA-iSP100 electron probe in the School of Earth and

**Table 1**

Summary of information relating to tephra horizons identified in the B53 and B54 ice cores. The depths are those for the particle peaks within the samples containing tephra.

Core	Depth (m)	Date	Age (BP)	Composition	Proposed Source	Correlations	In HolVol v1.0?	HolVol source	Prior latitude of injection	Revised latitude of injection	VSSI (TgS)	
B54	157.10	2911 BCE	4861	Rhyolite and basaltic andesite	Extra-Antarctic		Yes	Tropics	5° N		55.1	
B53	172.29	2362 BCE	4312	Andesite	Bellingshausen Is., S. Sandwich Is.		Yes	Southern Hemisphere	37° S	59° 25' S	0.2	
B53	169.61	2273 BCE	4223	Basaltic andesite	Saunders Is. or Visokoi Is., S. Sandwich Is.		Yes	Southern Hemisphere	37° S	57° S <sup>a</sup>	3.4	
B53	160.73	1994 BCE	3944	Andesite	Candlemas Is., S. Sandwich Is.		No					
B53	148.87	1632 BCE	3582	Andesite	Candlemas Is., S. Sandwich Is.		No					
B53	148.28*	1613 BCE	3563	Andesite	Candlemas Is., S. Sandwich Is.	Vostok tephra	Yes	Southern Hemisphere	37° S	57° S	0.8	
B54	121.86*	1612 BCE	3562	Andesite	Candlemas Is., S. Sandwich Is.	Vostok tephra	Yes	As above	As above	As above	"	
B53	142.02	1416 BCE	3366	Rhyolite	Extra-Antarctic		Yes	Southern Hemisphere	37° S		2.6	
B53	140.33	1364 BCE	3314	Dacite	S. Sandwich and/or S. Shetland Is.		Yes	Southern Hemisphere	37° S	60° S <sup>b</sup>	4.8	
G	B53	112.52	520 BCE	2470	Basaltic trachyandesite to basaltic andesite	Hudson volcano, South America	HW <sub>6</sub>	Yes	Southern Hemisphere	37° S	45° S	1.6
	B53	108.31	393 BCE	2343	Dacite	S. Sandwich Is.		Yes	Tropics	5° N	(58° S) <sup>c</sup>	15.8
B54	80.77	23 BCE	1973	Andesite	S. Shetland Is.		Yes	Southern Hemisphere	37° S	62° S <sup>d</sup>	2	
B53	95.17	21 BCE	1971	Basaltic andesite	S. Shetland Is.		Yes	As above	As above	As above	"	
B54	75.50	168 CE	1782	Basaltic andesite	S. Sandwich and/or S. Shetland Is.		Yes	Tropics	5° N	(60° S) <sup>e</sup>	12.4	
B53	85.54	245 CE	1705	Basaltic trachyandesite to basaltic andesite	Deception Is., S. Shetland Is.		No					
B53	46.88	1190 CE	760	Rhyolitic	Extra-Antarctic		Yes	Tropics	5° N		8.3	
B54	42.63	1252 CE	698	Trachyte	Mount Rittmann, Victoria Land	Rittmann tephra	No					

VSSI = HolVol volcanic stratospheric sulphur injections from [Sigl et al. \(2022\)](#). \*visible horizon.

<sup>a</sup> Latitude halfway between the islands.

<sup>b</sup> Latitude approximately halfway between the South Sandwich and South Shetland Islands.

<sup>c</sup> General latitude for the South Sandwich Islands - Latitude of injection for a proportion of the total sulphur for this event/year (see text for details).

<sup>d</sup> General latitude for the South Shetland Islands.

<sup>e</sup> Latitude approximately halfway between the South Sandwich and South Shetland Islands - Latitude of injection for a proportion of the total sulphur for this event/year (see text for details).

Environmental Sciences, University of St Andrews. To prepare the samples for BSE-EDS analysis they were polished for 1–2 min using 1 µm diamond paste prior to being carbon coated. Exposed particle surfaces were identified using BSE compositional imagery and possible tephra shards were isolated using the morphology of the particles, their

greyscale appearance and their live EDS spectra gained using a 1 µm electron beam diameter and a 5 nA beam current. Overall these investigations did not identify tephra shards to be further analysed, which will be discussed in Section 3.3.

Ages were assigned to any cryptotephra horizons based on the depth

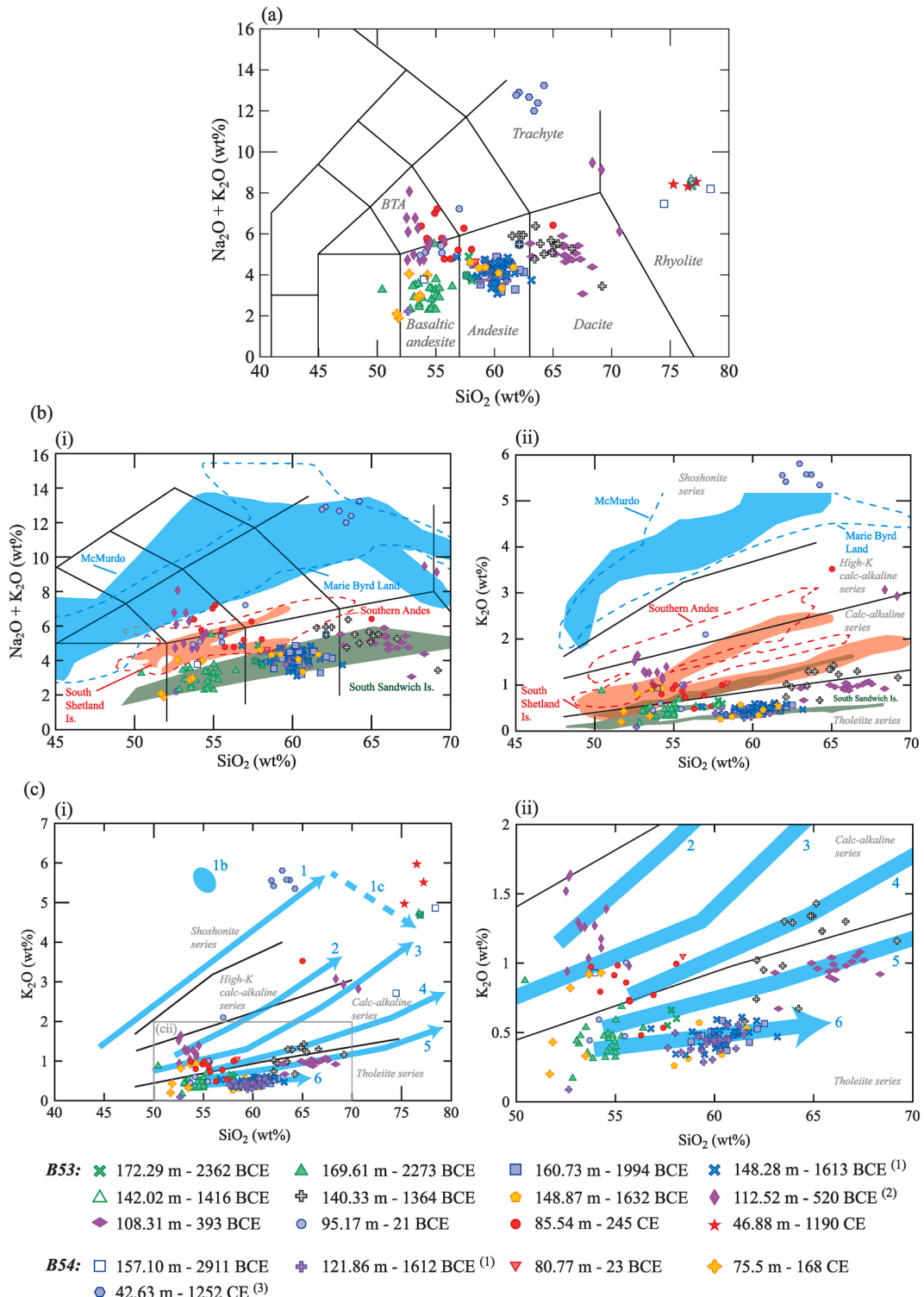


**Fig. 3.** Comparison of geochemical characterisations of individual glass shards from visible tephra and cryptotephra horizons in B53 and B54. Previously identified tephra horizons now isolated in B53 and/or B54: (1) Vostok tephra (2) HW<sub>6</sub> (3) Rittmann tephra. Chemical classification and nomenclature for total alkalis versus silica plot (a) after Le Bas et al. (1986). BTA = basaltic trachyandesite. Chemical classification and nomenclature for K<sub>2</sub>O v SiO<sub>2</sub> plot (b) after Peccerillo and Taylor (1976). Geochemical fields for the volcanic regions (b) from Narcisi et al. (2005) and references within. Geochemical lineages for regional volcanic sources (c) from Del Carlo et al. (2018), based on a compilation of geochemical characterisations of proximal deposits. See text for details on specific lineages of interest.

of the particle peak associated with the event and rounded to the nearest year downcore if required. The BCE/CE timescale used to assign dates to tephra includes a Year 0 and BP ages are given relative to 1950 CE (Table 1). Potential sources for the ice-core tephra horizons were explored through the comparison of the geochemical data from the individual glass shards to analyses of proximal deposits from volcanic regions of interest. When necessary, our datasets and those from literature sources were re-normalised with selected minor oxides (e.g.  $P_2O_5$ ,  $MnO$ ,  $Cl$ ) removed to ensure the same suite of elements was being compared between deposits. Statistical comparisons were made between tephra occurrences using the similarity coefficient (SC) function of Borchardt et al. (1972), with values greater than 0.95 indicating that samples can be regarded as identical (Beget et al., 1992), and the statistical distance ( $D^2$ ) test described in Perkins et al. (1995, 1998). To further assess the potential source of volcanic events the relative timing between the peak deposition of particles and the peak deposition of sulphur was considered. Approximately coeval peaks in both datasets implies rapid tropospheric transport of both tephra and sulphate, indicative of a local source, while a relative delay in peak sulphur deposition could indicate a more distal source due to delayed deposition of sulphate from the stratosphere (Koffman et al., 2017; Smith et al., 2020; Abbott et al., 2021b).

Lastly, we compared the timing of the events to eruptions in the HolVol v.1.0 database of Sigl et al. (2022). This database reports estimates of the magnitude and approximate source latitudes of major sulphur injecting volcanic eruptions over the Holocene, including 616 events in the last 5,500 years. It extends the eVolv2k database of Toohey and Sigl (2017) which provides the recommended volcanic forcing for all climate model simulations contributing to the Paleoclimate Modelling Intercomparison Project phase 4 (PMIP4) *past1000* simulations (Jungclaus et al., 2017). If any cryptotephra horizons for which we can identify a source have the same timing as events in the database, we can refine the latitude of sulphur injection. As an example, if the source attribution based on the cryptotephra analysis is consistent with the broad source in HolVol it may be possible to refine the latitude of injection based on the tephra source attribution. This then allows a

revision of the global radiative forcing potential of the eruptions as latitude is the key variable for converting polar sulphate deposition into atmospheric sulphate loading (Marshall et al., 2019; Plunkett et al., 2023). A more complex scenario arises if the source attribution based on the cryptotephra analysis is inconsistent with the broad source in the database. For example, if the tephra derives from a Southern Hemisphere volcanic source but the eruption in the database has been ascribed a tropical source based on bipolar sulphate deposition. This scenario has two possible explanations: 1) the Southern Hemisphere eruption was coeval with a Northern Hemisphere eruption and accounts for the sulphate deposition over Antarctica or 2) that the Southern Hemisphere eruption was coeval with a tropical eruption and contributed a proportion of the sulphate deposited over Antarctica.

### 3. Results

Overall, two visible tephra and 15 cryptotephra horizons have been identified across the two cores (Fig. 2; Table 1). Based on measurements of glass shards made using optical microscopy prior to geochemical analysis shard long axis lengths ranged between 10 and 50  $\mu m$  with most shards having lengths between 15 and 25  $\mu m$  (see Table S1 for grain-size information for individual horizons). The geochemical signatures of the tephra horizons are diverse and compositions include basaltic andesite, basaltic trachyandesite, andesite, dacite, trachyte and rhyolite (Fig. 3a) and many display affinities to the products of regional volcanic sources (Fig. 3b). The majority have relatively homogenous compositions, indicating that the shards derived from single volcanic eruptions; however, for a few horizons some geochemical heterogeneity can be observed. Three of the horizons have been identified previously in other Antarctic ice cores or palaeoclimatic sequences and will be discussed first (Section 3.1) before the remaining horizons are grouped and investigated based on their geochemical compositions (Section 3.2).

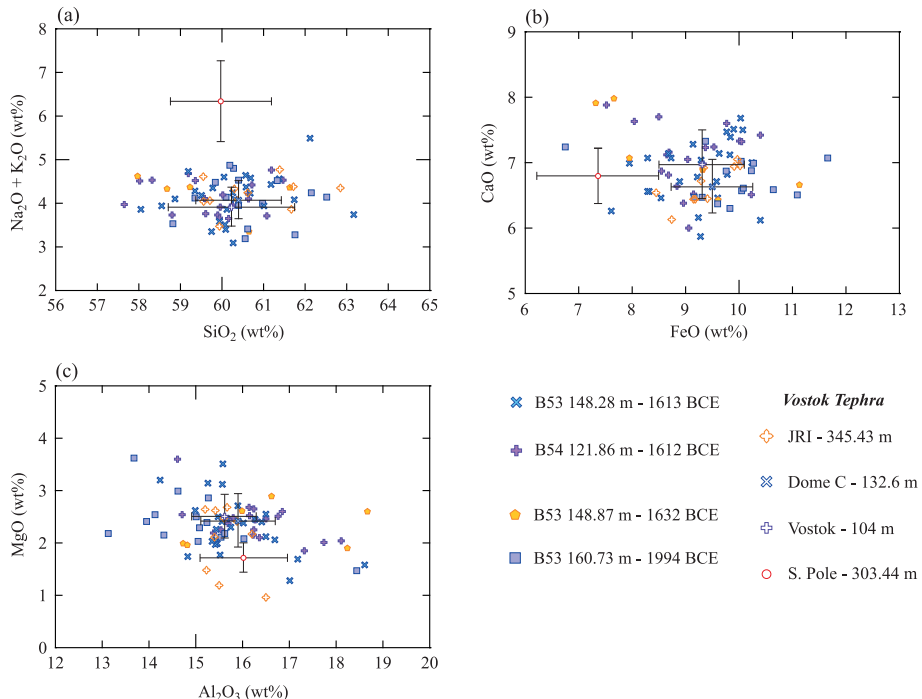


**Fig. 4.** Comparisons of geochemical characterisations of visible tephra layers in the B53 and B54 ice cores and selected geochemically similar horizons with characterisations of tephra layers from several Antarctic ice cores correlated as the Vostok tephra. Geochemical (microprobe glass analyses) data for the Vostok tephra occurrences from JRI (McConnell et al., 2021), Dome C (Narcisi et al., 2005), Vostok (Basile et al., 2001) and South Pole (Palais et al., 1987).

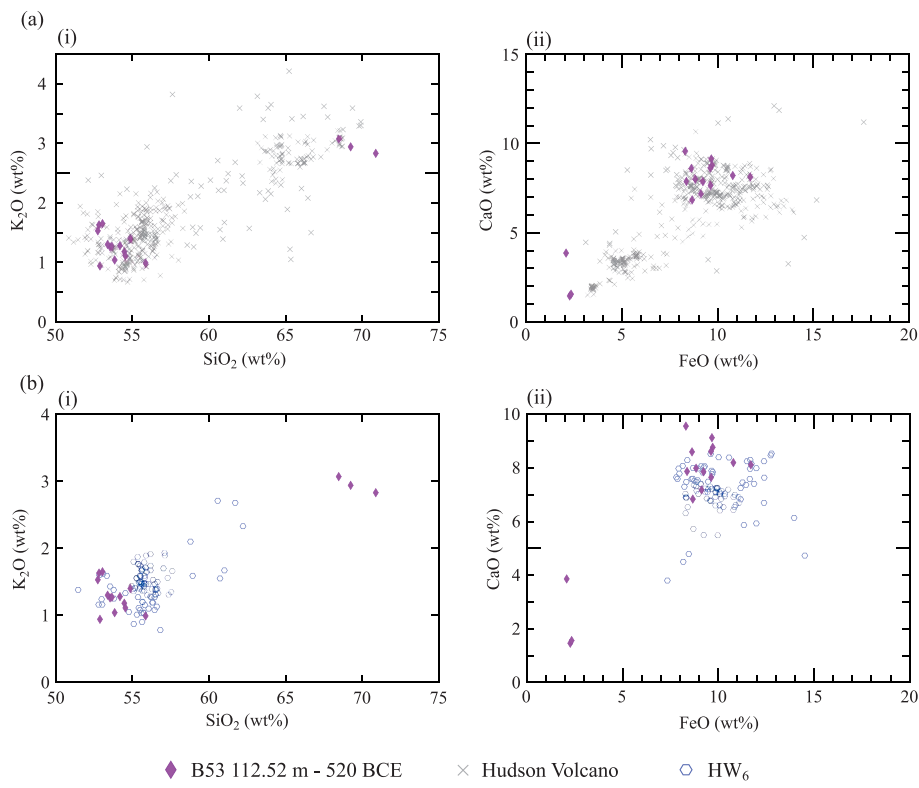


**Fig. 5.** Comparisons of the geochemical characterisation of the B53 112.52 m horizon to glass shards analyses of the products of (a) the Hudson volcano and (b) the HW<sub>6</sub> tephra horizon from [Haberle and Lumley \(1998\)](#).

### 3.1. Previously identified tephra horizons

#### 3.1.1. Vostok tephra

Visible tephra horizons have been identified in B53 and B54 at depths of 148.28 m and 121.86 m, respectively, and are dated to 1613 BCE and 1612 BCE ([Fig. 2](#)). Glass tephra shards from both horizons have an andesitic composition, a tholeiitic affinity due to their low K<sub>2</sub>O concentrations and strong similarities to the volcanic products of the South Sandwich Islands ([Fig. 3](#)). The chronological match and geochemical similarities between the two horizons indicate they can be correlated between the cores ([Fig. 4](#)). In addition, except for the older geochemical data for the South Pole occurrence, these geochemical characterisations are not statistically different and have strong similarities with glass shards from tephra layers contained within several ice cores from East Antarctica and the Antarctic Peninsula previously correlated as the Vostok tephra ([Fig. 4; Table S6](#)). The Vostok tephra was first identified in a shallow core from Vostok by [Kyle et al. \(1982, 1984\)](#) and later by [Basile et al. \(2001\)](#) in the deep Vostok core. This horizon is thought to be sourced from an eruption in the South Sandwich Islands and has a wide regional distribution, shown by its identification in a South Pole shallow core ([Palais et al., 1987](#)), the Dome C ice core ([Narcisi et al., 2005](#)) and, most recently, the James Ross Island ice core from the Antarctic Peninsula ([McConnell et al., 2021](#)). The identification of this horizon in B53 and B54 extends the known distribution of the Vostok tephra further across the interior of the EAIS ([Fig. 1](#)). Sulphur concentrations were not measured over these two horizons as the ice sections were cut out prior to the continuous chemical analyses. This was necessary due to the impact the high concentration of glass shards in the visible horizons could have on the analytical system. Moderate volcanic sulphate deposition dated to 1612 BCE has been recorded in other ice cores from across Antarctica ([Pearson et al., 2022; Sigl et al., 2022](#)).

#### 3.1.2. HW<sub>6</sub>, Hudson volcano

One horizon, B53 112.52 m, can be clearly defined as calc-alkaline ([Fig. 3bii](#)) and the individual shards display two populations, a main population between basaltic trachyandesite and basaltic andesite and a trachytic sub-population ([Fig. 3a](#)). There are some overlaps between the composition of B53 112.52 m and characterisations of the products of eruptions from the South Shetland Islands ([Fig. 3b](#)). However, comparison of the geochemical composition of this horizon to proximal material from regional volcanic sources highlights strong compositional similarities to the products of the Mount Hudson volcano in Chile, South America ([Fig. 5a](#)), and lineage 2 of [Del Carlo et al. \(2018\)](#), which they associate with the products of this source ([Fig. 3cii](#)). An additional similarity that can be observed is geochemical bimodality, a characteristic feature of the products of Mount Hudson ([Fig. 5a; Haberle and Lumley, 1998](#)). Specific similarities to the HW<sub>6</sub> horizon, identified by [Haberle and Lumley \(1998\)](#) in lakes west of Mount Hudson, can be observed ([Fig. 5b](#)). HW<sub>6</sub> was ascribed an age of 2740 cal yr BP using radiocarbon dating by [Haberle and Lumley \(1998\)](#), which is broadly comparable to the age of 520 BCE (2470 cal yr BP) we give to the B53 112.52 m horizon. Statistical distance comparisons of the geochemical compositions of the main population of B53 112.52 m and several HW<sub>6</sub> occurrences described in [Haberle and Lumley \(1998\)](#) demonstrate that they are not statistically different ([Table S7](#)). Relatively low SC values, ranging between 0.877 and 0.937, indicates some geochemical differences between the proximal and distal deposits despite the strong overlaps of the geochemical fields ([Fig. 5b](#)). This could be due, however, to the average compositions not representing the data well due to geochemical heterogeneity within both proximal and distal characterisations and the analysis of the two datasets on different microprobes. Overall, despite the slight geochemical differences, we propose a correlation between B53 112.52 m and HW<sub>6</sub> and this is supported by the chronological similarities between the age estimates for the horizons. The short time lag between the deposition of microparticles and sulphate for this event ([Fig. 6a](#)) is consistent with the suggested Mount

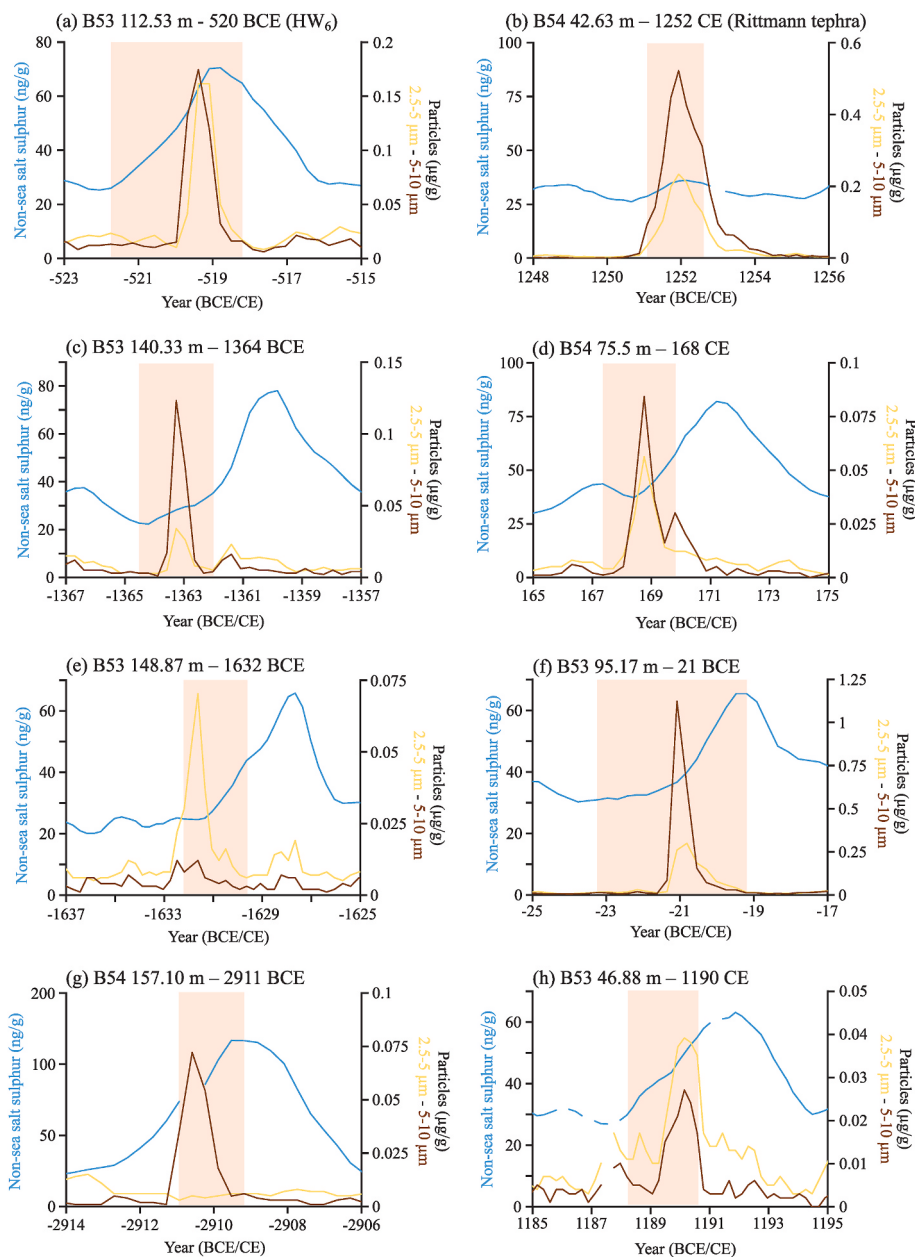


**Fig. 6.** Centimetre-resolution (~3–4 analyses per year resolution) non-sea-salt-sulphur and insoluble particle (2.5–5 µm and 5–10 µm diameter) records over volcanic events containing geochemically characterised glass tephra shards. Red bars denote the sample intervals containing glass tephra shards. Events are dated to (a) 520 BCE (b) 1252 CE (c) 1364 BCE (d) 168 CE (e) 1632 BCE (f) 21 BCE (g) 2911 BCE (h) 1190 CE.

Hudson source as the temporal relationship is typical for eruptions from relatively local sources.

### 3.1.3. Rittmann tephra

The cryptotephra identified at 42.63 m depth in B54 has a trachyte composition, unique within our framework (Fig. 3a). This composition is characteristic of the products of the Antarctic volcanoes of Marie Byrd Land and the McMurdo Volcanic Group (Fig. 3b) and clearly falls on lineage 1 of Del Carlo et al. (2018), which is the geochemical trend associated with the products of these sources (Fig. 3ci). The age of B54 42.63 m, 1252 CE, is consistent with the age of the Rittmann tephra, which was first identified in the Talos Dome ice core by Narcisi et al. (2001) and subsequently in the Siple and Taylor Dome ice cores by Dunbar et al. (2003) and the TALDICE core by Narcisi et al. (2012). A comprehensive analysis of this horizon is provided by Lee et al. (2019) who correlated occurrences in EAIS and WAIS ice cores from WAIS

Divide, RICE and the Styx Glacier and blue ice patches at Brimstone Peak and the Rennick Glacier in Victoria Land using major element chemistry (Fig. 1). This tephra can also be traced in regional marine records, with Di Roberto et al. (2019) first isolating the horizon as a cryptotephra in the BAY05-20c core from the Ross Sea and later studies identifying the horizon in other cores from the area (e.g. Tesi et al., 2020; Di Roberto et al., 2023). Both Lee et al. (2019) and Di Roberto et al. (2019) provide microprobe geochemical analyses of proximal glass tephra deposits from Mount Rittmann, but not specifically from the 1252 CE eruption, to confirm it was the source.

There are strong geochemical similarities between glass tephra shards from B54 42.63 m, the ice core, blue ice and marine occurrences of the Rittmann tephra and proximal deposits from Mount Rittmann (Fig. 7). For the similarity coefficient comparisons, 50 % have a SC > 0.95 and the remainder are >0.93 and the lower values for some comparisons could be attributed to the comparison of geochemical data from

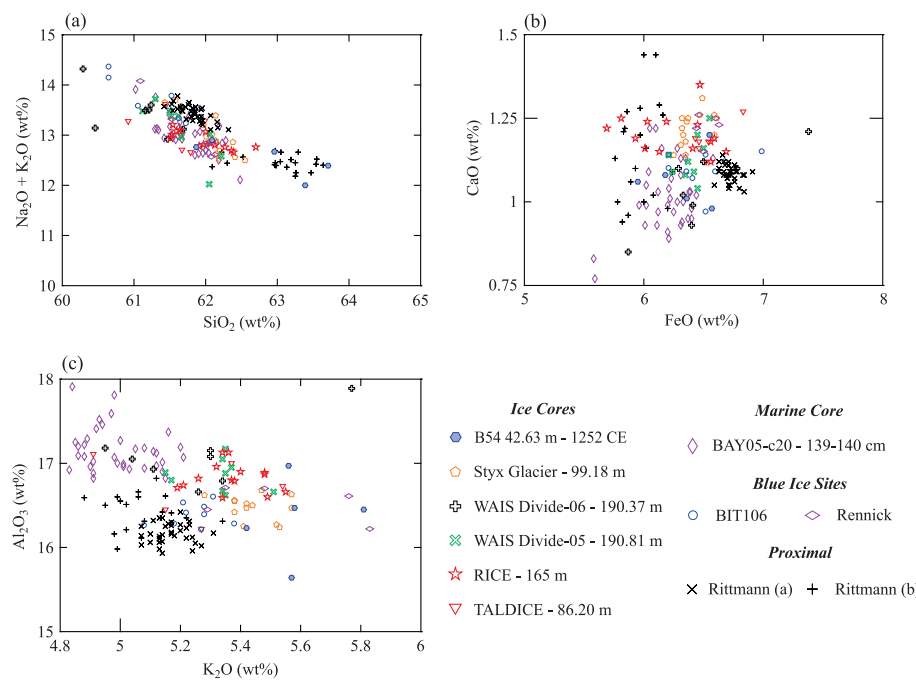


**Fig. 7.** Comparisons of the geochemical characterisation of B54 42.63 m to microprobe glass analyses from tephra occurrences correlated to an eruption of Mount Rittmann, Northern Victoria Land in 1252 CE and deposits proximal to the Mount Rittmann volcano. Geochemical data from TALDICE from [Narcisi et al. \(2012\)](#) and for BAY05-c20 and proximal Rittmann (b) from [Di Roberto et al. \(2019\)](#). All other data from [Lee et al. \(2019\)](#).

different microprobes ([Table S8](#)). Only the comparison between B54 42.63 m and data from the proximal Rittmann deposits presented in [Lee et al. \(2019\)](#) were found to be statistically different ([Table S8](#)), which could be attributed to the proximal deposits not deriving from this specific eruption. Overall, we can correlate B54 42.63 m with the Rittmann tephra significantly extending the known distribution of this tephra and representing its first identification in the interior of the EAIS. Based on the previously known distribution of the tephra, 2000 km from the source, [Lee et al. \(2019\)](#) concluded that it was potentially a Plinian eruption and the largest known Holocene eruption from the region. However, [Di Roberto et al. \(2019\)](#) proposed that the eruption of Mount Rittmann in 1252 CE was a long-lasting, explosive, but non-Plinian, eruption lower in magnitude than earlier eruptions of Mount Rittmann dated to ~11 ka BP (i.e. early Holocene) and ~22 ka BP ([Di Roberto et al., 2020; Torricella et al., 2021](#)). The widespread dispersal of ash following the 1252 CE eruption is attributed to sustained and prolonged emission of fine-grained ash and changes in wind direction during the eruption ([Di Roberto et al., 2019](#)). We extend the known distribution of ash to ~2900 km from Mount Rittmann, however, this can be regarded as a minimum estimate as this is the shortest possible pathway and a longer circum-polar atmospheric transport pathway is likely based on the prevailing wind direction over Antarctica. This finding further highlights that ash dispersal was widespread following the eruption but does not provide definitive insights into its magnitude, as widespread ash dispersal can occur following both high and relatively low intensity eruptions.

### 3.2. Newly identified tephra horizons

#### 3.2.1. Tholeiitic series deposits

Alongside the Vostok tephra several other horizons have homogeneous tholeiitic compositions which display clear affinities to the products of the South Sandwich Islands ([Fig. 3bii](#)). Two horizons, B53 148.87 m and B53 160.73 m, are geochemically similar to the andesitic Vostok tephra ([Fig. 4](#)), B53 172.29 m also has an andesite composition, B53 169.61 m has a basaltic andesite composition, and B53 108.31 m has a dacite composition ([Fig. 3a](#)). The compositions of these horizons

also all fall on lineages 6 and 5 of [Del Carlo et al. \(2018\)](#), which are associated with the products of this source. For most of these horizons the deposition of particles and sulphate was relatively coeval ([Figs. S1a-d](#)), consistent with a relatively local volcanic source for the eruptions.

The South Sandwich Islands are a volcanic arc along the eastern margin of the Scotia Sea comprising 11 volcanic islands, some of which were active during the Holocene period, and it has been a notable source of tephras deposited over East Antarctica over the last ~400 ka (e.g. [Baker, 1990; Narcisi and Petit, 2021](#)). Due to their remoteness and relative inaccessibility the proximal volcanic record of the islands is understudied ([Pearce et al., 1995; Liu et al., 2021](#)) and relatively limited geochemical characterisations and age estimates are available to aid the attribution of the horizons in our framework to specific volcanoes or eruptions.

Whole-rock geochemical analyses of volcanic rocks presented in [Pearce et al. \(1995\)](#) show that the different islands can be split into three distinct series, low-K tholeiitic, tholeiitic and calc-alkaline, with analyses from several islands falling along each trend ([Fig. 8a](#)). From our framework the compositions of the Vostok tephra, B53 148.87 m and B53 160.73 m fall on the trend of the low-K tholeiitic series ([Fig. 8a](#)). The closest compositional similarities for these horizons are with the products of Candlemas Island ([Fig. 8a and b](#)), which has been noted to exceptionally produce andesitic material ([Baker, 1990](#)) and was previously proposed as the source of the Vostok tephra ([Palais et al., 1987](#)). [Fig. 4](#) highlights the geochemical similarities between these older horizons and the Vostok tephra highlighting that Candlemas Island erupted prior to the event depositing the visible horizon. The compositions of B53 172.29 m and B53 169.61 m both fall on the trend of the tholeiitic series ([Fig. 8a](#)). While B53 172.29 m displays affinities to the products of Bellingshausen Island, which in general have higher SiO<sub>2</sub> concentrations than the other two islands in the tholeiitic series, B53 169.61 m displays a similar composition to the products of both Saunders and Visokoi Islands ([Fig. 8a and c](#)). B53 108.31 m could fall on the trend of the tholeiitic series proposed by [Pearce et al. \(1995\)](#) if it extended to higher SiO<sub>2</sub> values; however, no analyses of rocks from either Saunders, Bellingshausen or Visokoi Islands have a dacitic composition and SiO<sub>2</sub>

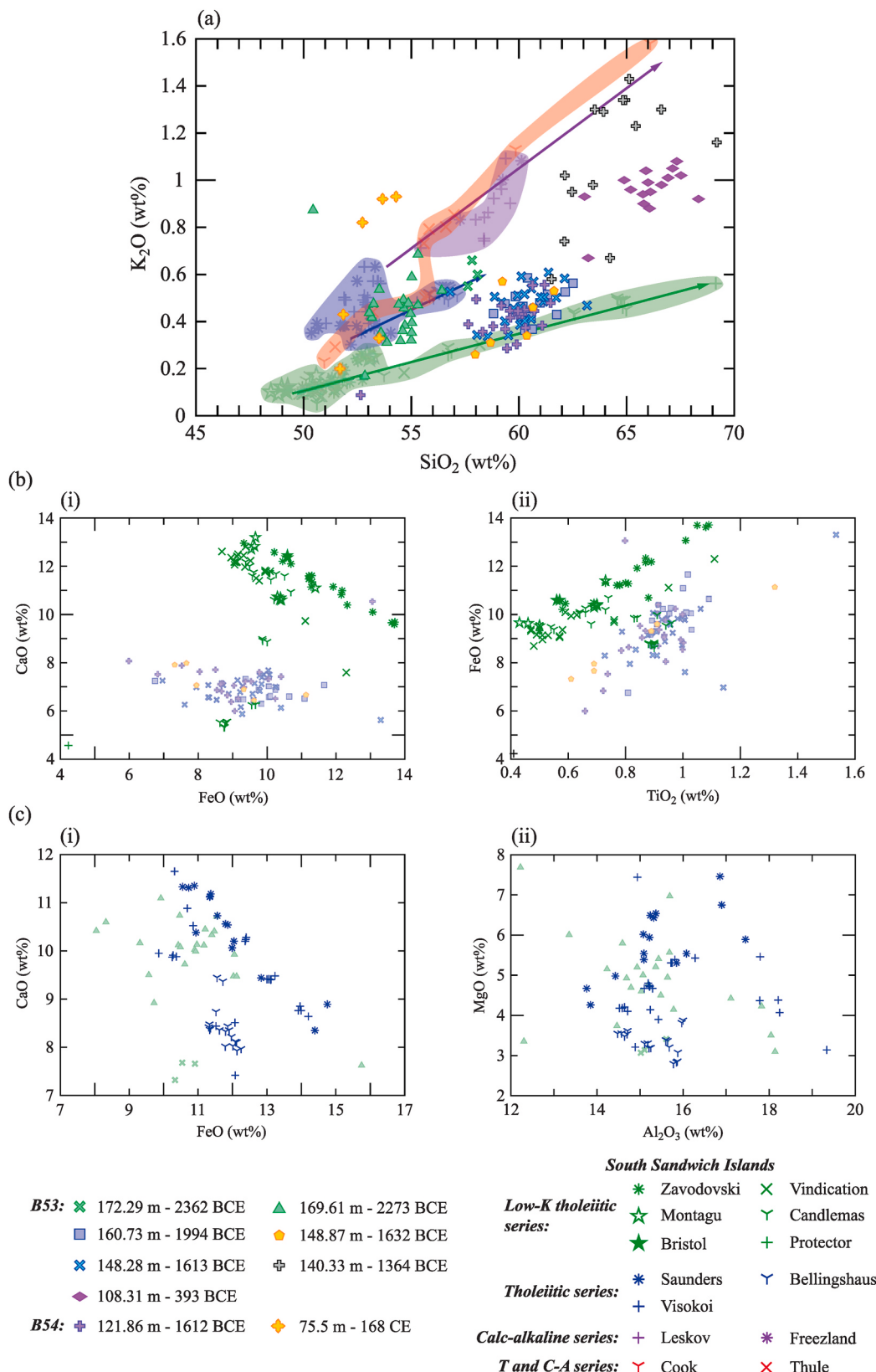


**Fig. 8.** (a) Geochemical composition of selected B53 and B54 tephra horizons compared to characterisations of proximal deposits from the South Sandwich Islands. (b) Comparison of low-K tholeiitic deposits from the B53 and B54 ice cores to proximal low-K tholeiitic material from the South Sandwich Islands. (c) Comparison of the characterisation of the tholeiitic B53 172.29 m and B53 169.61 m deposits with proximal tholeiitic material from the South Sandwich Islands. All South Sandwich Island whole-rock data and geochemical trends from Pearce *et al.* (1995).

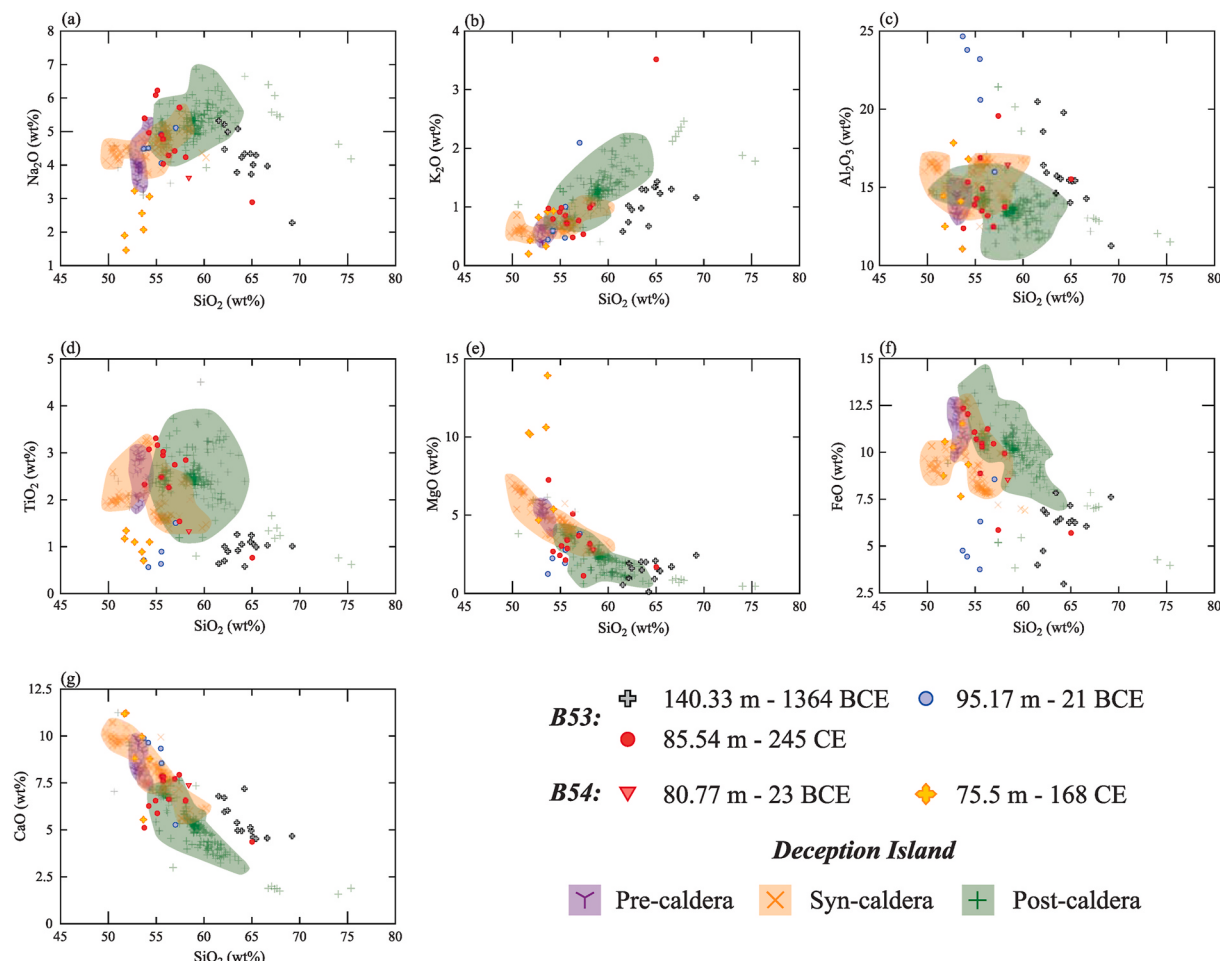


**Fig. 9.** (a–g) Geochemical compositions of selected B53 and B54 tephra horizons compared to microprobe analyses of glass from deposits proximal to Deception Island and deriving from pre-caldera, syn-caldera and post-caldera samples. Deception Island data from Geyer et al. (2019).

concentrations in excess of 65 wt% (Fig. 8a).

### 3.2.2. Deposits between the tholeiitic and calc-alkaline series

The geochemical signatures of four horizons, B54 75.50 m, B53 95.17 m, B53 85.54 m and B53 140.33 m, span the boundary between the tholeiite and calc-alkaline series on the K<sub>2</sub>O v SiO<sub>2</sub> biplot and a single analysis from B54 80.77 m falls within the calc-alkaline field (Fig. 3bii). These horizons display a range of compositions from basaltic andesite to dacite (Fig. 3a). The compositions of B53 95.17 m, B53 85.54 m and B54 80.77 m consistently fall within the geochemical envelopes of the products of the South Shetland Islands and not the Southern Andes due to their relatively lower K<sub>2</sub>O compositions (Fig. 3b). The analyses from B53 95.17 m generally fall on lineage 5 of Del Carlo et al. (2018) (Fig. 3cii), which is associated with the products of the South Sandwich Islands. However, as the total alkali concentrations of the ice core shards exceed those for South Sandwich Islands whole-rock analyses reported in Baker (1990) and Pearce et al. (1995) we correlate B53 95.17 m to the products of the South Shetland Islands. The analyses from B53 85.54 m fall between lineages 4 and 3, which are associated with products of the South Shetland Islands and Antarctic Peninsula volcanoes respectively and the analysis from B54 80.77 m falls on lineage 4 (Fig. 3cii).

The most likely source of tephra from the South Shetland Islands is Deception Island, which has been highly active during the Late Holocene and the reconstruction of past volcanic activity has been aided by studies of lacustrine sequences in the region (Björck et al., 1991b; Smellie, 1999). Recent work on the volcano provides two useful datasets for comparisons. Firstly, Geyer et al. (2019) provides a geochemical

database of proximal Deception Island deposits, including microprobe analyses of juvenile glass, they attribute to phases of formation before, during and after the caldera forming event most recently dated to 3980 ± 125 cal yr BP (Antoniades et al., 2018). Secondly, Hopfenblatt et al. (2022a) has compiled the DecTephra database, which contains published stratigraphic, geochemical and chronological information on 362 tephra layers, but not individual eruptions, thought to have been sourced from Deception Island over the past ~10 ka. A comparison of the composition of the ice-core deposits to analyses from Geyer et al. (2019) shows that for all major elements the composition of B53 85.54 m falls within the geochemical field of the Deception Island products and most closely the post-caldera analyses (Fig. 9). B53 85.54 m has been given an age of 245 CE (1705 a BP) using the WD2014 ice-core chronology and an inspection of the DecTephra database shows that it is most similar in age to the AP-6 tephra (Hopfenblatt et al., 2022b). This tephra was first identified in three lakes on the South Shetland Islands by Björck et al. (1991b) and has been ascribed an age of 1780–1920 yr BP based on radiocarbon dates from Walker Point, Elephant Island (Björck et al., 1991a; Hopfenblatt et al., 2022b). Subsequently Mulvaney et al. (2012) correlated a visible layer in the James Ross Island ice core, dated to 1730 ± 200 yr BP, to the AP-6 horizon. Despite these chronological similarities it is not possible to test the potential correlation between B53 85.54 m and the AP-6 tephra as a geochemical characterisation for AP-6 is not available for comparison.

A comparison of B53 95.17 m to microprobe glass analyses from Deception Island products reveals similar major element concentrations for SiO<sub>2</sub>, K<sub>2</sub>O and CaO, but distinct differences for Al<sub>2</sub>O<sub>3</sub> TiO<sub>2</sub> and FeO

values (Fig. 9). A comparison to major element data collated within the DecTephra database highlights similarities between the composition of B53 95.17 m and some analyses from marine cores in the Scotia Sea, downwind from the South Shetland Islands, reported by Moreton (1999) (Fig. 10). These high  $\text{Al}_2\text{O}_3$  analyses are from two layers of disseminated ash deposited during the last glacial period, but are outlying from the main populations that fall within the geochemical envelope of the Deception Island products (Fig. 10). As such, it is unlikely that B53 95.17 m derived from a Deception Island eruption, but most likely another local source within the South Shetland Islands. While Deception Island is the most active volcano in the South Shetland Islands several other volcanoes are in this area and the northern Antarctic Peninsula; however, they have not all been active during the Holocene (Smellie, 1990, 1999). Comparison of the composition of B53 95.17 m with glass analyses of rocks from a number of these volcanoes, presented in Kraus et al. (2013), does not highlight any potential sources with similarly high  $\text{Al}_2\text{O}_3$  values (Fig. 10). Therefore, at present, it is not possible to further refine the potential source of B53 95.17 m. Based on the age ascribed to B54 80.77 m, 23 BCE, and the one given to B53 95.17 m, 21 BCE, and timescale uncertainties of  $\sim \pm 1$  year at these depths, these horizons could be from the same event. The single analysis from B54 80.77 m shows general similarities to the analyses from B53 95.17 m (Fig. 9) so we assume they derive from the same event but additional geochemical evidence is required to test this proposition.

The relative heterogeneity of  $\text{K}_2\text{O}$  concentrations from the individual glass shards in B53 140.33 m and B54 75.50 m makes it difficult to determine relationships with the lineages of Del Carlo et al. (2018) and the most likely sources of these horizons. For example, there are similarities to the products of both the South Sandwich and South Shetland Islands (Fig. 3b). In addition, the linear trends on the  $\text{K}_2\text{O}$  v  $\text{SiO}_2$  plots are steeper than those generally observed for the lineages and the different geochemical series of the island groups (Figs. 3c and 8a). Whilst, overall, the characterisations are more heterogeneous than other deposits we have identified, the extent of heterogeneity for most oxides is most likely not sufficient to be attributable to secondary redeposition and the mixing of shards from multiple eruptions and sources. It is possible that the heterogeneity derives from the deposition of shards from two coeval eruptions and the geochemical bimodality that can be observed for some oxides, e.g.  $\text{K}_2\text{O}$  (Fig. 8a), is consistent with this proposition. Considering the characterisations as two separate populations would circumvent the need to account for the steep linear trend

on the  $\text{K}_2\text{O}$  v  $\text{SiO}_2$  plots. The apparent lag of  $\sim 2$  years between peak particle deposition and peak sulphate deposition for these horizons (Fig. 6c and d) could indicate that the deposits are derived from more distal volcanic regions. Alternatively, it could indicate that deposition of the different parameters was unrelated, with the particles deposited via reworking prior to deposition of sulphate from a volcanic eruption. However, a similar temporal relationship has been observed for other deposits more confidently attributed to primary tephra deposition from volcanic eruptions in the South Sandwich Islands (e.g. B53 148.87 m, Fig. 6e) and the South Shetland Islands (e.g. B53 95.17 m, Fig. 6f; B53 80.77 m, Fig. S1e). Overall, it cannot be definitively ruled out that these deposits were deposited via secondary reworking, however, we concur they most likely result from the deposition of tephra shards from two coeval eruptions from the South Sandwich Islands and/or the South Shetland Islands. Improved proximal characterisations and investigations of similarly timed deposits in ice cores from other sites may provide further evidence to resolve this issue.

### 3.2.3. Rhyolitic deposits

Within the tephra framework glass shard analyses with a rhyolitic composition were gained from four deposits (Fig. 3a). B53 46.55 m yielded three analyses of a rhyolitic composition and three were gained from B54 157.10 m alongside a single analysis of basaltic andesite composition. The only shard analysis gained from B53 142.02 m and an outlying shard from the main population of B53 172.29 m also have rhyolitic compositions (Fig. 3a). All the rhyolitic analyses, except for one analysis from B54 157.10 m, display a high-K composition (Fig. 3ci). These high-K rhyolitic analyses fall close to Lineage 1c defined by Del Carlo et al. (2018) as representing high-silica alkaline glasses erupted by intraplate volcanoes of West Antarctica. However, such eruptions are rare in Antarctica and last occurred during the Plio-Pleistocene, earlier than the time period considered in this study (e.g. Shane and Froggatt, 1992). The shards could derive from other sources surrounding Antarctica that have more recently and more regularly erupted rhyolitic material, such as the southern Andes and New Zealand (e.g. Del Carlo et al., 2018; Hopkins et al., 2021; Martínez Fontaine et al., 2023). Comparing the composition of microprobe glass analyses of material proximal to these sources to the rhyolitic shards from the ice core horizons highlights some geochemical similarities apart from two analyses from B53 46.88 m (Fig. 11). All the analyses share broad geochemical similarities with three rhyolitic horizons (TD341, TD655, TD667)

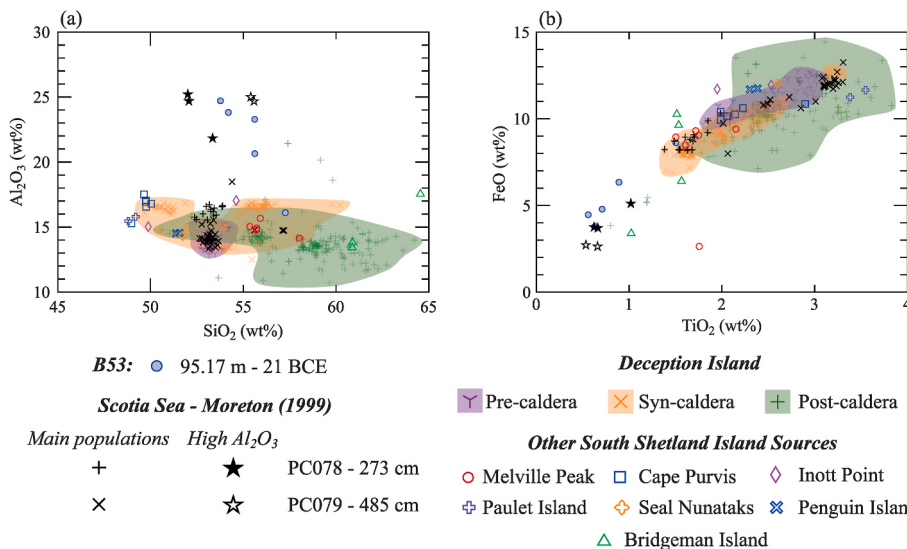


**Fig. 10.** Comparison between the geochemical composition of B53 95.17 m, microprobe analyses of glass from deposits proximal to Deception Island and other South Shetland Islands sources and geochemical analyses from two disseminated ash deposits from the Scotia Sea reported in Moreton (1999). Deception Island data from Geyer et al. (2019). Other South Shetland Islands glass analyses from Kraus et al. (2013).

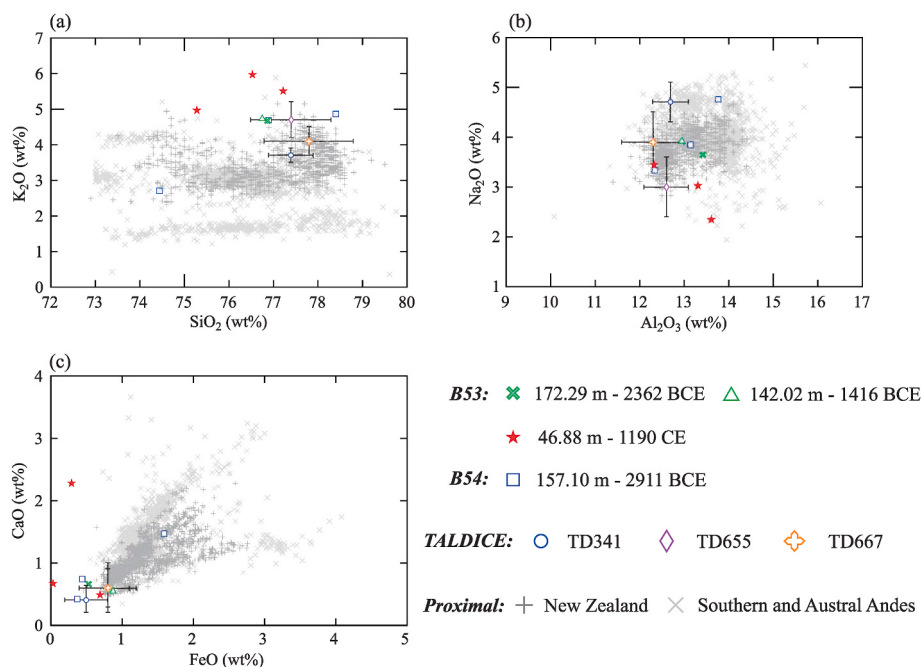


**Fig. 11.** Comparisons between the geochemical composition of rhyolitic glass shards from the B53 and B54 tephra horizons, microprobe glass analyses of proximal tephra deposits from New Zealand and the Southern and Austral Andes, from Hopkins et al. (2021) and Martínez Fontaine et al. (2023) respectively, and average and standard deviation values for selected rhyolitic horizons from Narcisi et al. (2012). Geochemical data from Martínez Fontaine et al. (2023) was screened to only include EPMA analyses of glass shards with >73 wt% SiO<sub>2</sub>. Data from Hopkins et al. (2021) for the Tuhua tephra has been excluded from the plots.

identified in the TALDICE core (Fig. 11; Narcisi et al., 2012). Narcisi et al. (2012) concluded that these horizons derived from volcanic sources outside Antarctica, with the Andes suggested as the most likely source, however, New Zealand was not ruled out. Further analysis to identify a specific volcanic source for the horizons yielding three analyses, B54 157.10 m and B53 46.88 m dated to 2911 BCE and 1190 CE respectively, is hindered by the distinct heterogeneity between the analyses (Fig. 11). The heterogeneity may derive from the shards not being from a single volcanic eruption or analytical challenges related to the small size of the tephra shards. Overall, we suggest that the rhyolitic glass shards in B53 and B54 were most likely sourced from extra-Antarctic volcanic regions but further analysis would be required to more definitively ascertain their source. The relationship between particle and sulphate deposition for B54 157.10 m and B53 46.88 m does not contradict this assertion, with a small temporal lag between peak particle and sulphate deposition potentially indicative of distal eruption sources (Fig. 6g and h).

### 3.3. Additional tephra investigations of significant volcanic signals

Identifying the source of some specific volcanic events recorded as chemical signals in these Antarctic cores has wider importance for reconstructing past volcanism and its impact over the Mid-to Late Holocene. As such, a selection of samples were additionally assessed using a SEM approach to determine if they contained glass tephra shards smaller than those identified using optical microscopy, which could have an effective limit of  $\sim 10 \mu\text{m}$  diameter as shards smaller than this were not identified during the initial analysis. Samples from B53 and/or B54 for volcanic events in 1809 CE, 1458 CE, 1276 CE, 1268 CE, 1257 CE, 434 CE, 236 CE, 427 BCE and 2911 BCE were selected as events with unknown, potentially tropical, volcanic sources and/or related to significant climatic changes. In addition, except for the sample from 2911 BCE, no glass tephra shards were identified in these samples during initial optical microscopy. This additional analysis did not identify glass shards in any of the samples, thus it was not possible to further explore and identify the source of the selected volcanic events using cryptotephra

analysis. Possible explanations for the lack of tephra shards in the samples associated with these events and potential avenues for further investigating these presumed tropical eruptions will be discussed further in Section 4.2.

### 3.4. Comparison of tephra source attributions to Holocene eruption database

Comparison of the timing of the cryptotephras we have identified in the Antarctic ice core records to HolVol v1.0 shows that of the 15 volcanic events we have analysed, four are not in the database as they did not produce enough sulphur to be identified as major sulphur injecting volcanic eruptions. Notably, the eruption in 1252 CE that deposited the Rittmann tephra over a large area of Antarctica is amongst these events, consistent with the limited sulphate deposition associated with this event in B54 (Fig. 6b). The remaining events relate to sulphur injecting eruptions in the database and could help refine the eruption parameters for these events. Analysis of these 11 events shows that nine have source attributions consistent between the sulphate and cryptotephra analysis. Based on the tephra analysis we can refine the latitude of sulphur injection for some of these events that have more robust source attributions (Table 1). For example, B53 112.52 m, deposited in 520 BCE, relates to an eruption in the HolVol database of Sigl et al. (2022) that was ascribed a source in the Southern Hemisphere as a coeval sulphate peak was not identified in Greenland. The identification of Mount Hudson as the source of the tephra confirms the attribution of Sigl et al. (2022) and the latitude of sulphur injection can be refined from 37°S, the default latitude assigned to all unidentified extratropical Southern Hemisphere eruptions, to 45°S, the latitude of Mount Hudson (Table 1). In addition, several sulphate deposition events that were related to Southern Hemisphere eruptions can now be linked to eruptions from the South Sandwich Islands and/or the South Shetland Islands (Table 1). For the three events we classified as having a source beyond Antarctica, B54 157.10 m, B53 142.02 m and B53 46.88 m, the injection latitudes from the database are consistent, however, we cannot refine the latitudes without improved tephra-based source attributions.

For tephra horizons B53 108.31 m and B54 75.50 m deposited in 393 BCE and 168 CE, respectively, there is some contradiction between the source attributions based on the sulphate and cryptotephra analysis. Our tephra evidence suggests eruptions occurred within the Southern Hemisphere during those years whilst evidence for bipolar sulphate deposition reported in Sigl et al. (2022) led them to conclude that the eruptions were tropical. As highlighted earlier, this could result from an eruption occurring in either the Northern Hemisphere or the tropics during the same year as a Southern Hemisphere eruption. If the relative contributions of sulphate from the two eruptions can be disentangled then our tephra evidence provides an injection latitude for the Southern Hemisphere eruption (Table 1).

For all years containing volcanic events Sigl et al. (2022) report the volcanic stratospheric sulphur injection (VSSI), which can be used as a measure of the potential climatic impact of the eruption or eruptions during that year. For the six eruptions we can confidently attribute to Southern Hemisphere sources VSSIs values range between 0.2 and 4.8 TgS (Table 1; Sigl et al., 2022). These values are less than 10 times the sulphur ejected by the Northern Hemisphere Okmok 43 BCE eruption ( $48 \pm 16$  TgS; McConnell et al., 2020; Abbott et al., 2021a) and are unlikely to have had a significant impact on Southern Hemisphere climate. At present, the lack of a reliable annually resolved temperature record for the Southern Hemisphere does not allow us to fully assess this proposition (Anchukaitis and Smerdon, 2022). For the years 393 BCE and 168 CE, during which we infer that both a Southern Hemisphere and either a Northern Hemisphere or tropical eruption, occurred the VSSIs were greater, 15.8 and 12.4 TgS respectively (Sigl et al., 2022). However, it is not possible to determine the relative contribution of sulphur from the Southern Hemisphere eruptions to the overall VSSIs for these years, and consequentially possible climate impacts, without further investigations. For the three events assigned extra-Antarctic sources, two had relatively minor VSSIs with 2.6 and 8.3 TgS emitted from the events in 1416 BCE and 1190 CE respectively. The third event in 2911 BCE had a large VSSI of 55.1 TgS, the 15th largest VSSI during the Holocene, and tree-ring evidence suggests it could have caused a climatic cooling (Salzer et al., 2014; Sigl et al., 2022). Further work is required to gain more analyses of tephra shards from Antarctic ice cores to determine the source of the tephra deposited over Antarctica and to determine if that eruption contributed towards cooling around 2911 BCE.

#### 4. Discussion

##### 4.1. Contribution of mid-to late Holocene tephra framework towards reconstructing volcanic history

Overall, our work represents a significant improvement to the tephrochronological record for the interior of the EAIS over the Mid-to Late Holocene, providing initial tephra geochemical characterisations for 12 volcanic events and extending the known geographical distribution of tephra deposition for three previously characterised events. These tephra horizons can now be used as tie-lines and chronostratigraphic markers if they can be traced within other palaeoclimatic archives. Most of the newly characterised events are from volcanic regions relatively proximal to the core sites, i.e. the South Sandwich and South Shetland Islands, aiding the reconstruction of volcanism from these sources. These characterisations and the age estimates based on the ice-core chronology could help guide future proximal investigations in these regions which may also help refine our source attributions.

A notable feature of the timing of the events we have characterised is a relative dominance of eruptions from the South Sandwich Islands between 2362 BCE to 393 BCE before events from the South Shetland Islands dominate between 23 BCE and 245 CE (Table 1). This could be due to changes in eruptive activity of the volcanic centres or a temporal shift in atmospheric dispersal patterns affecting which sources dominantly deposited tephra over the core sites. These factors could be

investigated further by comparing the timing to shifts in palaeowind reconstructions and proximal volcanic records. For individual volcanic centres there is a distinct period of activity from Candlemas Island in the South Sandwich Islands with two eruptions occurring within 400 years before the eruption forming the Vostok tephra. We assume that the youngest event has the largest magnitude due to the widespread deposition of tephra as a visible deposit across the Antarctic Peninsula and the EAIS. Only one eruption from the South Shetland Islands could be attributed to a specific source, the highly productive Deception Island. It is, however, noteworthy that a tephra layer from the caldera-forming eruption of Deception Island was not identified in B53 and/or B54 despite the core sites downwind locations and as the most recent age for the event,  $3980 \pm 125$  cal yr BP, falls within our window of investigation (Antoniades et al., 2018). Estimates of the age of this event have ranged between the late Pleistocene and 3370 yr BP and an age of 10 kyr BP has often been quoted (see Antoniades et al., 2018). While we cannot provide further evidence for the age of the event, we do not consider that our non-identification calls into question the most recent age. Other factors such as wind patterns at the time of the eruption, the topography of the surface snow and/or a lack of a sulphate signal from the eruption could have contributed towards the non-identification of tephra from this specific eruption at the core sites.

Our source attributions could be refined through the improvement of major element datasets for comparison from proximal deposits, which at present are limited for certain sources due to the relative inaccessibility of the volcanic regions. In addition, for all potential sources the attribution of horizons to specific volcanoes could be improved by gaining trace element characterisations from the glass tephra shards in the ice-core horizons. This analysis would provide additional chemical constraints on the eruptive source for the eruptions, which can show greater variation between individual volcanoes than major element analyses and for a number of centres proximal trace element characterisations have already been gained (e.g. Baker, 1990; Kraus et al., 2013; Del Carlo et al., 2018). For example, it could help to identify sources for the B53 140.33 m and B54 75.50 m horizons for which it was not possible to determine if they originated from the South Sandwich Islands, the South Shetland Islands or coeval eruptions from both sources. Shard specific trace element analyses have previously been gained from glass tephra shards isolated in ice cores from both Greenland and Antarctica (e.g. Basile et al., 2001; Kohno et al., 2004; Abbott et al., 2012; Bourne et al., 2016; Plunkett et al., 2017; Cook et al., 2022) but, at present, it is not routinely utilised. This is due to analytical challenges relating to the typically small size of tephra shards extracted from ice cores, the destructive nature of the method, the low concentrations of shards typically present in deposits and, to date, limited testing of inter-comparability of trace element characterisations between laboratories (Pearce et al., 2011, 2014; Wallace et al., 2022). It could, however, be possible to apply trace element analysis to selected horizons of specific interest and visible horizons composed of larger glass shards and the issue of laboratory inter-comparability is currently being addressed by the community (Wallace et al., 2022). We recommend that any trace element analysis of distal tephra horizons could be coupled with efforts to further characterise both the major and trace element compositions of proximal deposits, to improve source attributions and define correlations between specific proximal and distal deposits.

It was postulated that the methodological approach utilised in this work may result in the identification of cryptotephras from the Antarctic volcanic sources of the McMurdo Volcanic Group and volcanoes protruding through the WAIS, which based on proximal records, are known to have been active during the Mid-to Late Holocene. However, only one eruption from these sources, the previously characterised Rittmann tephra, was identified in the studied cores. The identification of this tephra highlights that it is possible to trace cryptotephras from these sources into the interior of the EAIS, however, it is likely that tephra deposition over the interior of the EAIS from the Antarctic volcanoes is rare and our methodological approach may also constrain their

identification. The magnitude of the eruptions and extent of tephra dispersal from these sources may be too low to result in the deposition of tephra over the EAIS, even as cryptotephras. In addition, if these eruptions emit low levels of sulphur during eruptions our sampling strategy, focused on coeval particle and sulphur peaks, may lead to these events being overlooked. The sulphur and particle records over the Rittmann tephra highlight this potential issue as a very limited peak in sulphur is associated with this eruption (Fig. 6b).

The most distal proposed source for a tephra horizon in our framework is B53 112.52 m, which we correlate to the HW<sub>6</sub> tephra horizon from Mount Hudson, South America. South America has previously been proposed as a source of tephra horizons identified in Antarctica, however, it is acknowledged that these correlations have been challenged (Del Carlo et al., 2018), and B53 112.52 m does display some geochemical similarities to less distal sources, i.e. the South Shetland Islands. As such, the geochemical correlation between B53 112.52 m and HW<sub>6</sub> could be further tested through trace element analysis. If the HW<sub>6</sub> horizon can be traced in other Antarctic ice cores, medial sites between Mouth Hudson and Antarctica and proximally the robustness of this correlation could be increased, the atmospheric pathway facilitating the transport of ash to the site identified and the magnitude of the eruption constrained. This is important as the magnitude of the eruption depositing HW<sub>6</sub> is currently unknown, but it is not thought to have been a high-magnitude eruption, i.e. > VEI 6, and its geochemical composition does not indicate it was a highly explosive eruption.

In general, despite the focus on cryptotephra horizons, the sources of the tephras identified in this study are similar to those identified in other ice cores from the interior of the EAIS within studies focused on visible horizons and longer timescales (e.g. Palais et al., 1989; Kohno et al., 2004, 2005; Narcisi et al., 2005). Therefore, while we have not definitively identified tephra horizons from more distal sources than prior studies, the focus on identifying cryptotephras has resulted in tephra horizons being identified with a far higher temporal frequency than prior studies.

#### 4.2. Assessing current methodologies and future outlooks

Our study represents the first time the approach of tracing cryptotephras using coeval sulphate and particle peaks has been applied to create a tephrochronological framework for Antarctic ice cores, following its successful application within Greenland (Plunkett et al., 2023). This methodology contrasts with the arguably more time intensive approach of contiguous sampling at a lower resolution over time periods of interest (e.g. Bourne et al., 2015; Cook et al., 2022). The latter approach has the advantage that tephra horizons without an associated chemical peak can be identified, which is of use for reconstructing long-term volcanic history, but is less applicable when exploring the climatic impact of individual eruptions. We identified tephra horizons within ~20 % of the samples we assessed, which, is a greater rate of identification than most studies using the continuous approach (Abbott et al., 2012). The use of two cores was a great benefit within the construction of this tephra framework as, except for the visible Vostok tephra and one possible correlation, all cryptotephra horizons were only identified in one core despite 16 common events being sampled. This highlights the role site-specific factors, such as patchy deposition of tephra shards at distal sites, topographic differences in the surface snow and wind reworking, might play within the deposition and preservation of low concentrations of fine-grained tephra shards. However, it should also be noted that primarily potential tropical events were targeted during the sampling of the B54 core resulting in fewer events from this core being investigated and a lower likelihood of cryptotephra identification (see Section 2). Despite this, the addition of other cores to the network and more complete sampling of records in future studies could improve the overall framework and provide source information for further eruptions, including events sampled in this study for which an associated tephra deposit was not identified.

The methodological approach we undertook assumes that the particle record acts as an indicator for tephra deposition but despite a relatively high rate of success our analysis methods did not lead to the identification of glass tephra shards in every sample. For some particle peaks a cryptotephra population might not have been identified if any glass tephra shards present were too small, i.e.  $\lesssim 5 \mu\text{m}$  diameter, to be identified using the optical and microprobe methods we utilised. Such glass shards would, however, be large enough to be measured using the particle detector, as this can measure particles in the 1–10  $\mu\text{m}$  size range. Notably, with the exception of B53 148.87 m (Fig. 6e), all the cryptotephras we identified can be associated with a particle peak in the 5–10  $\mu\text{m}$  size range (Fig. 6 and S1) suggesting a particle peak in this size range is required for glass shards to be identified using our current methods. It is possible to utilise geochemical methods with a 1  $\mu\text{m}$  spatial resolution, such as EPMA, SEM-EDS or Fourier transform infrared imaging (FTIR), to analyse all particles in samples, including those  $<5 \mu\text{m}$  in diameter, to determine if glass tephra shards are present (e.g. Iverson et al., 2017; Malek et al., 2019; Narcisi et al., 2019). These approaches, however, necessitate a reduction of the accuracy and precision of the analytical data produced for characterisations, which could seriously hamper comparisons to datasets from proximal deposits and consequently defining correlations to volcanic sources.

Assessing the success rate of tephra identification and current methodologies links to an ambitious goal of this work, which was to provide source information for several eruptions thought to originate from tropical sources. Despite the use of additional methods aiming to increase our cryptotephra identification rate for fine-grained deposits from more distal sources (Section 3.3), no tephra horizons from tropical sources could be identified and our tephra record is dominated by eruptions from local extra-tropical sources (Table 1). This is consistent with past investigations of Antarctic ice cores (see Section 1) and highlights that despite the contrasting focus on cryptotephras instead of visible horizons we have not identified any new and/or more distal potential source areas. In the context of investigations of Greenland ice cores, Plunkett et al. (2023) highlights how poleward dispersal of tephra shards from tropical sources might be restricted by rapid settling and aggregation of ash particles of a size that can be identified and analysed using current methods and the altitude of injection required for longer residence times not being achieved. These factors are also applicable to Antarctica and could restrict the transport of ash from tropical eruptions and tephra transport could also be blocked by atmospheric features such as the polar vortex and the jet stream that lie between the tropics and poles. Therefore, it is possible that ash from the past tropical eruptions we have investigated was not deposited over the ice sheet. Equally, it is also possible that the typical size range of any tropical tephra shards is too small to be identified using our methodological approach (see examples in Koffman et al., 2013) and/or the concentration of shards deposited over Antarctica is very low and spatially heterogenous. In addition to the methods mentioned earlier small tephra shards could be searched for using existing continuous single particle analytical techniques, such as coupled CFA inductively coupled time of flight mass spectrometry (CFA-icpTOF; Erhardt et al., 2019). This method has the potential to measure both major and trace element compositions of individual particles in ice samples. However, before it can be routinely applied significant developmental steps would need to be made, firstly, to determine if glass tephra shards are being analysed and, secondly, to produce geochemical characterisations that could be directly compared to proximal analyses. Increasing the cross-sectional area of samples may aid the identification of tephra from tropical sources if deposition is at low concentrations and/or patchy in nature. The development and use of automated techniques for tephra identification would be advantageous in this context as increasing the cross-sectional area of samples would increase sample volumes and the overall number of particles to be inspected. In addition, as CFA-icpTOF can also characterise the elemental concentrations of non-tephra particles (Erhardt et al., 2019) it might be possible to determine the composition of particle peaks not

found to contain tephra.

#### 4.3. Contribution towards improved understanding of volcanic forcing during the mid-to late Holocene

Comparison of our tephra record to a database of Holocene eruptions, used to reconstruct the global radiative forcing potential of eruptions over this period, allowed us to refine sulphur injection latitudes for several eruptions (Section 3.4; Table 1). For some of the eruptions, e.g. B53 140.33 m, B53 108.31 m and B54 80.77 m, approximate latitude estimates are given and further refinements could be possible if the specific source volcanoes can be identified through additional geochemical investigations (see Section 4.1). Such investigations may also allow specific sources, and thus injection latitudes, to be identified for the three rhyolitic horizons, assumed to have an extra-Antarctic source, from which a limited number of geochemical analyses were gained (Table 1; Fig. 11). Additionally, we identified potential complexity within two time intervals, around 393 BCE and 168 CE, where there is inconsistency between the tephra evidence and sulphate records. Further investigations could improve our understanding of volcanic activity during those time periods and determine whether the Southern Hemisphere eruption was coeval with a Northern Hemisphere eruption or a tropical eruption. For example, tephra analysis of ice cores from Greenland might provide evidence for a Northern Hemisphere eruption and sulphur isotope analysis of ice from both poles could be used as contrasting isotopic signatures would be expected in the different scenarios (Burke et al., 2019, 2023).

Comparisons with the Holocene database further highlighted that our tephra framework is skewed towards local volcanism as we could only provide refined eruption parameters for Southern Hemisphere eruptions. In addition, VSSI estimates for many of the eruptions we can provide a source for indicate that they were unlikely to have significantly impacted Southern Hemisphere climate. Refining eruption parameters for tropical eruptions through the identification of associated tephra might only be possible following the development of new methodological approaches for tephra analysis (see Section 4.2), which could be applied to further exploring the source of the eruption in 2911 BCE. It should, however, be acknowledged that ash from specific tropical eruptions might not have been deposited over the Antarctic ice sheet. Assessing the potential for tephra to be deposited over Antarctica following tropical eruptions from different sources, of different magnitudes and under different atmospheric regimes (e.g. winter v summer) using ash transport models could help explore this issue. This could also identify the possible size range of any glass shards that might be deposited over the region and whether certain areas of the ice sheet could be the focus for future coring efforts due to a greater likelihood of preserving ash from tropical eruptions.

#### 5. Conclusions

Cryptotephra investigations underpinned by a sampling strategy focussed on co-occurring sulphate and microparticle peaks and an analytical protocol for the analysis of fine-grained glass tephra shards have been conducted on two Antarctic ice cores covering the Mid-to Late Holocene. These investigations have led to the identification of 15 cryptotephra horizons and the analysis of a visible tephra horizon common between the two cores. Three of the tephra horizons can be correlated to deposits previously identified in other palaeoclimatic archives and using their geochemical fingerprints and comparisons to proximal deposits possible volcanic sources have been identified for the remaining horizons. Similar to past studies of tephra horizons in ice cores from the interior of the EAIS the South Sandwich and South Shetland Islands are key sources for tephra horizons in these cores but horizons have also been correlated to sources in Victoria Land, Antarctica and South America. This new tephra framework contributes towards our understanding of the regional volcanic history. For

example, the identification of new occurrences of the three previously known tephra horizons extends the known geographical extent of tephra deposition for these events. In addition, a shift over time in the relative dominance of eruptions from the South Sandwich Islands to the South Shetland Islands could be indicative of changes in eruptive activity or atmospheric dispersal patterns. A comparison of the timing of the tephra horizons to the HolVol v1.0 database shows that 11 of the volcanic eruptions depositing tephra over Antarctica can be related to sulphur injections and based on source attributions the latitude of injection can be refined for six of the events. For the remaining five events further work is required to either improve tephra-based source attributions or determine if a Northern Hemisphere or a tropical eruption occurred coevally with the Southern Hemisphere eruption. An assessment of the magnitude of the sulphur injections related to all the eruptions suggests, that except for the event in 2911 BCE, they were unlikely to have had a significant impact on Southern Hemisphere climate.

Overall, this work represents a crucial first step towards improving the volcanic history of the Southern Hemisphere and refining the location of atmospheric sulphur injections from volcanic eruptions during the Mid-to Late Holocene and estimates of their radiative forcing potential. Building on past studies our findings further highlight how the identification and characterisation of cryptotephra in ice cores is a powerful tool for advancing our understanding of past volcanism when combined with high-resolution chemical records from these archives. This study, however, has highlighted a potential limitation that, despite the focus on cryptotephra horizons and with additional investigations of a subset of samples, with timings similar to major tropical eruptions, the records are dominated by ash from regional volcanic sources and no tephra from tropical sources was identified. These observations are consistent with past studies focused solely on visible tephra horizons and highlight that other approaches, beyond our cryptotephra approach, might be required to identify such events. This issue could be further explored through an increase in the cross-sectional area of samples and/or development of additional micro-analytical techniques, such as FTIR or CFA-icpTOF. These investigations, however, should be coupled with modelling efforts to determine the likelihood, possible size range and potential geographical spread of tephra deposition over Antarctica following tropical eruptions.

#### Author contributions

All authors contributed towards this manuscript. PA wrote the manuscript. PA and MS devised the study and the methodological approach. PA, EC and WH contributed towards tephra analysis and data interpretation. PA and MS conducted comparisons to the HolVol database. JM, NC and MS contributed ice-core glaciochemical records. SK, MH and JF were involved in the collection of the B53 and B54 ice cores and provided access for sampling. All authors provided comments and approve the submission.

#### Declaration of competing interest

The authors declare that they have no known competing financial interests or personal relationships that could have appeared to influence the work reported in this paper.

#### Data availability

Data will be made available on request.

#### Acknowledgements

PA and MS received funding from the European Research Council under the European Union's Horizon 2020 research and innovation programme (grant agreement no. 820047). WH is funded by a UKRI Future Leaders Fellowship (MR/S033505/1). Continuous analysis of the

B53 and B54 cores for sulphur and insoluble particles was supported by internal funding from the Desert Research Institute, with partial support for interpretation provided by National Science Foundation grant 1925417 to JRM. We thank the German field team for collecting the cores, as well as students and staff in the DRI ice-core group for assistance in the laboratory. Thanks to Pierre Lanari, Coralie Vesin and Hugo Dominguez Carranza for assistance with EPMA analysis at the University of Bern. Thanks to Gill Plunkett for comments on the manuscript. We thank two anonymous reviewers for their comments on the manuscript. This research benefitted from the participation of some of the authors in the Volcanic Impacts on Climate and Society (VICS) working group of the Past Global Changes (PAGES) project.

## Appendix A. Supplementary data

Supplementary data to this article can be found online at <https://doi.org/10.1016/j.quascirev.2024.108544>.

## References

- Abbott, P.M., Davies, S.M., 2012. Volcanism and the Greenland ice-cores: the tephra record. *Earth Sci. Rev.* 115 (3), 173–191.
- Abbott, P.M., Davies, S.M., Steffensen, J.P., Pearce, N.J.G., Bigler, M., Johnsen, S.J., Seierstad, I.K., Svensson, A., Wastegård, S., 2012. A detailed framework of Marine Isotope Stage 4 and 5 volcanic events in two Greenland ice-cores. *Quat. Sci. Rev.* 36, 59–77.
- Abbott, P.M., Niemeier, U., Timmreck, C., Riede, F., McConnell, J.R., Severi, M., Fischer, H., Svensson, A., Toohey, M., Reinig, F., Sigl, M., 2021a. Volcanic climate forcing preceding the inception of the Younger Dryas: implications for tracing the Laacher See eruption. *Quat. Sci. Rev.* 274, 107260.
- Abbott, P.M., Plunkett, G., Corona, C., Chellman, N.J., McConnell, J.R., Pilcher, J.R., Stoffel, M., Sigl, M., 2021b. Cryptotephra from the Icelandic Veðivötn 1477 CE eruption in a Greenland ice core: confirming the dating of volcanic events in the 1450s CE and assessing the eruption's climatic impact. *Clim. Past* 17, 565–585.
- Anchukaitis, K.J., Smerdon, J.E., 2022. Progress and uncertainties in global and hemispheric temperature reconstructions of the Common Era. *Quat. Sci. Rev.* 286, 107537.
- Antoniades, D., Giralt, S., Geyer, A., Álvarez-Valero, A.M., Pla-Rabes, S., Granados, I., Liu, E.J., Toro, M., Smellie, J.L., Oliva, M., 2018. The timing and widespread effects of the largest Holocene volcanic eruption in Antarctica. *Sci. Rep.* 8, 17279.
- Baker, P., 1990. E. South Sandwich islands. In: LeMasurier, W., Thomson, J., Baker, P., Kyle, P., Rowley, P., Smellie, J., Verwoerd, W. (Eds.), *Volcanoes of the Antarctic Plate and Southern Oceans*, vol. 48. Antarctic Research Series, pp. 360–395.
- Basile, I., Petit, J.R., Touren, S., Grousset, F.E., Barkov, N., 2001. Volcanic layers in Antarctic (Vostok) ice cores: source identification and atmospheric implications. *J. Geophys. Res.* 106, 31915–31931.
- Beget, J., Mason, O., Anderson, P., 1992. Age, extent and climatic significance of the c. 3400 BP Aniakchak tephra, western Alaska, USA. *Holocene* 2, 51–56.
- Bigler, M., Svensson, A., Steffensen, J.P., Kaufmann, P., 2007. A new continuous high-resolution detection system for sulphate in ice cores. *Ann. Glaciol.* 45, 178–182.
- Björck, S., Malmér, N., Hjort, C., Sandgren, P., Ingólfsson, O., Wallén, B., Smith, R.I.L., Jónsson, B.L., 1991a. Stratigraphic and paleoclimatic studies of a 5500-year-old moss bank on elephant island, Antarctica. *Arct. Alp. Res.* 23, 361–374.
- Björck, S., Sandgren, P., Zale, R., 1991b. Late Holocene tephrochronology of the northern antarctic Peninsula. *Quat. Res.* 36, 322–328.
- Boyd, J.A., Bingham, R.G., Ashmore, D.W., Karlsson, N.B., Hein, A.S., Vaughan, D.G., 2021. Age-depth stratigraphy of pine island glacier inferred from airborne radar and ice-core chronology. *J. Geophys. Res.* 126, e2020JF005927.
- Boyd, J.A., Bingham, R.G., Young, D.A., MacGregor, J.A., Ashmore, D.W., Quartini, E., Hein, A.S., Vaughan, D.G., Blankenship, D.D., 2023. High mid-Holocene accumulation rates over West Antarctica inferred from a pervasive ice-penetrating radar reflector. *Cryosphere* 17, 1497–1512.
- Borchardt, G.A., Aruscavage, P.J., Millard, H., 1972. Correlation of the Bishop ash, a Pleistocene marker bed, using instrumental neutron activation analysis. *J. Sediment. Petrol.* 42, 201–206.
- Bourne, A.J., Cook, E., Abbott, P.M., Seierstad, I.K., Steffensen, J.P., Svensson, A., Fischer, H., Schüpbach, S., Davies, S.M., 2015. A tephra lattice for Greenland and a reconstruction of volcanic events spanning 25–45 ka b2k. *Quat. Sci. Rev.* 118, 122–141.
- Bourne, A.J., Abbott, P.M., Albert, P.G., Cook, E., Pearce, N.J.G., Ponomareva, V., Svensson, A., Davies, S.M., 2016. Underestimated risks of recurrent long-range ash dispersal from northern Pacific Arc volcanoes. *Sci. Rep.* 6, 29837.
- Büntgen, U., Smith, S.H., Wagner, S., Krusic, P., Esper, J., Piermattei, A., Crivellaro, A., Reinig, F., Tegel, W., Kirdyanov, A., Trnka, M., Oppenheimer, C., 2022. Global tree-ring response and inferred climate variation following the mid-thirteenth century Samalas eruption. *Clim. Dynam.* 59, 531–546.
- Burke, A., Moore, K.A., Sigl, M., Nita, D.C., McConnell, J.R., Adkins, J.F., 2019. Stratospheric eruptions from tropical and extra-tropical volcanoes constrained using high-resolution sulfur isotopes in ice cores. *Earth Planet. Sci. Lett.* 521, 113–119.
- Burke, A., Innes, H.M., Crick, L., Anchukaitis, K.J., Byrne, M.P., Hutchison, W., McConnell, J.R., Moore, K.A., Rae, J.W.B., Sigl, M., Wilson, R., 2023. High sensitivity of summer temperatures to stratospheric sulfur loading from volcanoes in the Northern Hemisphere. *Proc. Natl. Acad. Sci. USA* 120, e2221810120.
- Cook, E., Abbott, P.M., Pearce, N.J.G., Mojtabavi, S., Svensson, A., Bourne, A.J., Rasmussen, S.O., Seierstad, I.K., Vinther, B.M., Harrison, J., Street, E., Steffensen, J.P., Wilhelms, F., Davies, S.M., 2022. Volcanism and the Greenland ice cores: a new tephrochronological framework for the last glacial-interglacial transition (LGIT) based on cryptotephra deposits in three ice cores. *Quat. Sci. Rev.* 292, 107596.
- Davies, S.M., 2015. Cryptotephra: the revolution in correlation and precision dating. *J. Quat. Sci.* 30, 114–130.
- DeConto, R.M., Pollard, D., 2016. Contribution of Antarctica to past and future sea-level rise. *Nature* 531, 591–597.
- Del Carlo, P., Di Roberto, A., D'Orazio, M., Petrelli, M., Angioletti, A., Zanchetta, G., Maggi, V., Daga, R., Nazzari, M., Rocchi, S., 2018. Late Glacial-Holocene tephra from southern Patagonia and Tierra del Fuego (Argentina, Chile): a complete textural and geochemical fingerprinting for distal correlations in the Southern Hemisphere. *Quat. Sci. Rev.* 195, 153–170.
- Di Roberto, A., Albert, P.G., Colizza, E., Del Carlo, P., Di Vincenzo, G., Gallerani, A., Giglio, F., Kuhn, G., Macrì, P., Manning, C.J., Melis, R., Misericocchi, S., Scateni, B., Smith, V.C., Torricella, F., Winkler, A., 2020. Evidence for a large-magnitude Holocene eruption of Mount Rittmann (Antarctica): a volcanological reconstruction using the marine tephra record. *Quat. Sci. Rev.* 250, 106629.
- Di Roberto, A., Colizza, E., Del Carlo, P., Petrelli, M., Finocchiaro, D., Kuhn, G., 2019. First marine cryptotephra in Antarctica found in sediments of the western Ross Sea correlates with glaciogenic tephras and climate records. *Sci. Rep.* 9, 10628.
- Di Roberto, A., Re, G., Scateni, B., Petrelli, M., Tesi, T., Capotondi, L., Morigi, C., Galli, G., Colizza, E., Melis, R., Torricella, F., Giordano, P., Giglio, F., Gallerani, A., Gariboldi, K., 2023. Cryptotephra in the marine sediment record of the edisto inlet, Ross Sea: implications for the volcanology and tephrochronology of the northern Victoria Land, Antarctica. *Quaternary Science Advances* 10, 100079.
- Dunbar, N.W., Iverson, N.A., Van Eaton, A.R., Sigl, M., Alloway, B.V., Kurbatov, A.V., Mastin, L.G., McConnell, J.R., Wilson, C.J.N., 2017. New Zealand supereruption provides time marker for the Last Glacial Maximum in Antarctica. *Sci. Rep.* 7, 12238.
- Dunbar, N.W., Kurbatov, A.V., 2011. Tephrochronology of the Siple Dome ice core, West Antarctica: correlations and sources. *Quat. Sci. Rev.* 30, 1602–1614.
- Dunbar, N.W., Zielinski, G.A., Voisins, D.T., 2003. Tephra layers in the Siple Dome and Taylor Dome ice cores, Antarctica: sources and correlations. *J. Geophys. Res.* 108, 2374.
- Erhardt, T., Jensen, C.M., Borovinskaya, O., Fischer, H., 2019. Single particle characterization and total elemental concentration measurements in polar ice using continuous flow analysis-inductively coupled plasma-time-of-flight mass spectrometry. *Environ. Sci. Technol.* 53, 13275–13283.
- Fujii, Y., Kohno, M., Motoyama, H., Matoba, S., Watanabe, O., Fujita, S., Azuma, N., Kikuchi, T., Fukuo, T., Suzuki, T., 1999. Tephra layers in the Dome Fuji (Antarctica) deep ice core. *Ann. Glaciol.* 29, 126–130.
- Gautier, E., Savarino, J., Hoek, J., Erbland, J., Caillon, N., Hattori, S., Yoshida, N., Albala, E., Albareda, F., Farquhar, J., 2019. 2600-years of stratospheric volcanism through sulfate isotopes. *Nat. Commun.* 10, 466.
- Geyer, A., Álvarez-Valero, A.M., Gisbert, G., Aulinás, M., Hernández-Barreña, D., Lobo, A., Martí, J., 2019. Deciphering the evolution of Deception Island's magmatic system. *Sci. Rep.* 9, 373.
- Guillet, S., Corona, C., Oppenheimer, C., Lavigne, F., Khodri, M., Ludlow, F., Sigl, M., Toohey, M., Atkins, P.S., Yang, Z., Muranaka, T., Horikawa, N., Stoffel, M., 2023. Lunar eclipses illuminate timing and climate impact of medieval volcanism. *Nature* 616, 90–95.
- Haberle, S.G., Lumley, S.H., 1998. Age and origin of tephras recorded in postglacial lake sediments to the west of the southern Andes, 44°S to 47°S. *J. Volcanol. Geoth. Res.* 84, 239–256.
- Hall, M., Hayward, C., 2014. Preparation of micro- and crypto-tephras for quantitative microbeam analysis. In: Austin, W.E.N., Abbott, P.M., Davies, S.M., Pearce, N.J.G., Wastegård, S. (Eds.), *Marine Tephrochronology*, vol. 398. Geological Society of London Special Publication, pp. 21–28.
- Hartman, L.H., Kurbatov, A.V., Winski, D.A., Cruz-Uribe, A.M., Davies, S.M., Dunbar, N.W., Iverson, N.A., Aydin, M., Fegyveresi, J.M., Ferris, D.G., Fudge, T.J., Osterberg, E.C., Hargreaves, G.M., Yates, M.G., 2019. Volcanic glass properties from the 1459 C.E. volcanic event in South Pole ice core dismiss Kuwae caldera as a potential source. *Sci. Rep.* 9, 14437.
- Hopfenblatt, J., Geyer, A., Aulinás, M., Álvarez-Valero, A.M., Polo Sánchez, A., Giralt, S., Smellie, J.L., 2022a. DecTephra: a new database of Deception Island's tephra record (Antarctica). *J. Volcanol. Geoth. Res.* 425, 107516.
- Hopfenblatt, J., Geyer, A., Aulinás, M., Álvarez-Valero, A.M., Polo Sánchez, A., Giralt, S., Smellie, J.L., 2022b. Database of deception Island's tephra record (DecTephra) (v.1.0). Zenodo. <https://doi.org/10.5281/zenodo.6077062>.
- Hopkins, J.L., Bidmead, J.E., Lowe, D.J., Wysoczanski, R.J., Pillans, B.J., Ashworth, L., Rees, A.B.H., Tuckett, F., 2021. TephraNZ: a major- and trace-element reference dataset for glass-shard analyses from prominent Quaternary rhyolitic tephras in New Zealand and implications for correlation. *Geochronology* 3, 465–504.
- Iverson, N.A., Kalteyer, D., Dunbar, N.W., Kurbatov, A., Yates, M., 2017. Advancements and best practices for analysis and correlation of tephra and cryptotephra in ice. *Quat. Geochronol.* 40, 45–55.
- Jacob, R.W., Welch, B.C., 2005. A time marker at 17.5 kyr BP detected throughout West Antarctica. *Ann. Glaciol.* 41, 47–51.
- Jensen, B.J.L., Pyne-O'Donnell, S., Plunkett, G., Froese, D.G., Hughes, P.D.M., Sigl, M., McConnell, J.R., Amesbury, M.J., Blackwell, P.G., van den Bogaard, C., Buck, C.E., Charman, D.J., Clague, J.J., Hall, V.A., Koch, J., Mackay, H., Mallon, G., McCall, L.,

- Pilcher, J.R., 2014. Transatlantic distribution of the alaskan white river ash. *Geology* 42, 875–878.
- Jungclaus, J.H., Bard, E., Baroni, M., Braconnor, P., Cao, J., Chini, L.P., Egorova, T., Evans, M., Gonzalez-Rouco, J.F., Goosse, H., Hurt, G.C., Joos, F., Kaplan, J.O., Khodri, M., Goldewijk, K.K., Krivova, N., LeGrande, A.N., Lorenz, S.J., Luterbacher, J., Man, W.M., Maycock, A.C., Meinshausen, M., Moberg, A., Muscheler, R., Nehrbass-Ahles, C., Otto-Biesner, B.I., Phipps, S.J., Ponratz, J., Rozanov, E., Schmidt, G.A., Schmidt, H., Schmutz, W., Schurer, A., Shapiro, A.I., Sigl, M., Smerdon, J.E., Solanki, S.K., Timmreck, C., Toohey, M., Usoskin, I.G., Wagner, S., Wu, C.J., Yeo, K.L., Zanchettin, D., Zhang, Q., Zorita, E., 2017. The PMIP4 contribution to CMIP6-Part 3: the last millennium, scientific objective, and experimental design for the PMIP4 past1000 simulations. *Geosci. Model Dev. (GMD)* 10, 4005–4033.
- Koffman, B.G., Dowd, E.G., Osterberg, E.C., Ferris, D.G., Hartman, L.H., Wheatley, S.D., Kurbatov, A.V., Wong, G.J., Markle, B.R., Dunbar, N.W., Kreutz, K.J., Yates, M., 2017. Rapid transport of ash and sulfate from the 2011 Puyehue-Cordón Caulle (Chile) eruption to West Antarctica. *J. Geophys. Res.* 122, 8908–8920.
- Koffman, B.G., Kreutz, K.J., Kurbatov, A.V., Dunbar, N.W., 2013. Impact of known local and tropical volcanic eruptions of the past millennium on the WAIS Divide microparticle record. *Geophys. Res. Lett.* 40, 4712–4716.
- Kohno, M., Fujii, Y., Hirata, T., 2004. Chemical composition of volcanic glasses in visible tephra layers found in a 2503 m deep ice core from Dome Fuji, Antarctica. *Ann. Glaciol.* 39, 576–584.
- Kohno, M., Kipfstuhl, S., Lambrecht, A., Fujii, Y., Kronz, A., 2005. Tephra study on the EPICA-DML ice core. *Geophys. Res. Abstr.* 7, 07573.
- Kraus, S., Kurbatov, A., Yates, M., 2013. Geochemical signatures of tephras from quaternary Antarctic Peninsula volcanoes. *Andean Geol.* 40, 1–40.
- Kuehn, S.C., Froese, D.G., 2010. Tephra from ice – a simple method to routinely mount, polish, and quantitatively analyze sparse fine particles. *Microsc. Microanal.* 16, 218–225.
- Kurbatov, A.V., Zielinski, G.A., Dunbar, N.W., Mayewski, P.A., Meyerson, E.A., Sneed, S.B., Taylor, K.C., 2006. A 12,000 year record of explosive volcanism in the Siple Dome ice core, west Antarctica. *J. Geophys. Res.* 111, D12307.
- Kyle, P.R., Jezek, P.A., Mosley-Thompson, E., Thompson, L.G., 1981. Tephra layers in the Byrd Station ice core and the Dome C ice core, Antarctica and their climatic importance. *J. Volcanol. Geoth. Res.* 11, 29–39.
- Kyle, P.R., Palais, J., Delmas, R., 1982. The volcanic record of Antarctic ice cores: preliminary results and potential for future investigations. *Ann. Glaciol.* 3, 172–177.
- Kyle, P.R., Palais, J., Thomas, E., 1984. Vostok tephra – an important englacial stratigraphic marker? *Antarctic Journal* 64–65.
- Lane, C.S., Andric, M., Cullen, V.L., Blockley, S.P.E., 2011. The occurrence of distal Icelandic and Italian tephra in the Lateglacial of Lake Bled, Slovenia. *Quat. Sci. Rev.* 30, 1013–1018.
- Lavigne, F., Degeai, J.-P., Komorowski, J.-C., Guillet, S., Robert, V., Lahitte, P., Oppenheimer, C., Stoffel, M., Vidal, C.M., Surono, Pratomo, I., Wassmer, P., Hajdas, I., Hadmoko, D.S., de Belizal, E., 2013. Source of the great AD. 1257 mystery eruption unveiled, Samalas volcano, Rinjani Volcanic Complex. *Proc. Natl. Acad. Sci. USA* 110, 16742–16747.
- Le Bas, M.J., Le Maitre, R.W., Streckeisen, A., Zanettin, B., 1986. A chemical classification of volcanic rocks based on the total alkali-silica diagram. *J. Petrol.* 27, 745–750.
- Lee, M.J., Kyle, P.R., Iverson, N.A., Lee, J.I., Han, Y., 2019. Rittmann volcano, Antarctica as the source of a widespread  $1252 \pm 2$  CE tephra layer in Antarctic ice. *Earth Planet. Sci. Lett.* 521, 169–176.
- Liu, E.J., Wood, K., Aiuppa, A., Giudice, G., Bitetto, M., Fischer, T.P., McCormick Kilbride, B.T., Plank, T., Hart, T., 2021. Volcanic activity and gas emissions along the South Sandwich arc. *Bull. Volcanol.* 83, 3.
- Malek, M.A., Eom, H.-J., Hwang, H., Hor, S.D., Hong, S., Hou, S., Ro, C.-U., 2019. Single particle mineralogy of microparticles from Himalayan ice-cores using SEM/EDX and ATR-FTIR imaging techniques for identification of volcanic ash signatures. *Chem. Geol.* 504, 205–215.
- Marshall, L., Johnson, J.S., Mann, G.W., Lee, L., Dhomse, S.S., Regayre, L., Yoshioka, M., Carslaw, K.S., Schmidt, A., 2019. Exploring how eruption source parameters affect volcanic radiative forcing using statistical emulation. *J. Geophys. Res. Atmos.* 124, 964–985.
- Martínez Fontaine, C., Peña-Araya, V., Marmo, C., Le Morvan, M., Delpech, G., Fontijne, K., Siani, G., Cosyn-Wexsteen, L., 2023. Boom! Tephrochronological dataset and exploration tool of the Southern ( $33^{\circ}$ – $46^{\circ}$ S) and Austral ( $49^{\circ}$ – $55^{\circ}$ S) volcanic zones of the Andes. *Quat. Sci. Rev.* 316, 108254.
- Maselli, O.J., Chellman, N.J., Grieman, M., Layman, L., McConnell, J.R., Pasteris, D., Rhodes, R.H., Saltzman, E.S., Sigl, M., 2017. Sea ice and pollution-modulated changes in Greenland ice core methanesulfonate and bromine. *Clim. Past* 13, 39–59.
- McConnell, J.R., Burke, A., Dunbar, N.W., Köhler, P., Thomas, J.L., Arienzio, M.M., Chellman, N.J., Maselli, O.J., Sigl, M., Adkins, J.F., Baggenstos, D., Burkhardt, J.F., Brook, E.J., Buizert, C., Cole-Dai, J., Fudge, T.J., Knorr, G., Graf, H.F., Grieman, M., Iverson, N., McGwire, K.C., Mulvaney, R., Paris, G., Rhodes, R.H., Saltzman, E.S., Severinghaus, J.P., Steffensen, J.P., Taylor, K.C., Winckler, G., 2017. Synchronous volcanic eruptions and abrupt climate change similar to 17.7 ka plausibly linked by stratospheric ozone depletion. *Proc. Natl. Acad. Sci. USA* 114 (38), 10035–10040.
- McConnell, J.R., Chellman, N.J., Mulvaney, R., Eckhardt, S., Stohl, A., Plunkett, G., Kipfstuhl, S., Freitag, J., Isaksson, E., Gleason, K.E., Brugger, S.O., McWethy, D.B., Abram, N.J., Liu, P., Aristarain, A.J., 2021. Hemispheric black carbon increase after the 13<sup>th</sup>-century Māori arrival in New Zealand. *Nature* 598, 82–85.
- McConnell, J.R., Lamorey, G.W., Lambert, S.W., Taylor, K.C., 2002. Continuous ice-core chemical analyses using inductively coupled plasma mass spectrometry. *Environ. Sci. Technol.* 36 (1), 7–11.
- McConnell, J.R., Sigl, M., Plunkett, G., Burke, A., Kim, W.M., Raible, C.C., Wilson, A.I., Manning, J.G., Ludlow, F.M., Chellman, N.J., Innes, H.M., Yang, Z., Larsen, J.F., Schaefer, J.R., Kipfstuhl, S., Mojtabavi, S., Wilhelms, F., Opel, T., Meyer, H., Steffensen, J.P., 2020. Extreme climate after massive eruption of Alaska's Okmok volcano in 43 BCE and effects on the late Roman Republic and Ptolemaic Kingdom. *Proc. Natl. Acad. Sci. USA* 117, 15443–15449.
- Medley, B., McConnell, J.R., Neumann, T.A., Reijmer, C.H., Chellman, N., Sigl, M., Kipfstuhl, S., 2018. Temperature and snowfall in western Queen Maud Land increasing faster than climate model projections. *Geophys. Res. Lett.* 45, 1472–1480.
- Moreton, S.G., 1999. Quaternary Tephrochronology of the Scotia Sea and Bellinghausen Sea, Antarctica. PhD, University of Gloucestershire, Cheltenham.
- Mulvaney, R., Abram, N.J., Hindmarsh, R.C.A., Arrowsmith, C., Fleet, L., Triest, J., Sime, L.C., Alemany, O., Foord, S., 2012. Recent Antarctic Peninsula warming relative to Holocene climate and ice-shelf history. *Nature* 489, 141–144.
- Narcisi, B., Petit, J.R., Neumann, T.A., Reijmer, C.H., Chellman, N., Sigl, M., Kipfstuhl, S., 2018. Temperature and snowfall in western Queen Maud Land increasing faster than climate model projections. *Geophys. Res. Lett.* 45, 1472–1480.
- Narcisi, B., Petit, J.R., 2021. Englacial tephras of East Antarctica. In: Smellie, J.L., Panter, K.S., Geyer, A. (Eds.), *Volcanism in Antarctica: 200 Million Years of Subduction, Rifting and Continental Break-Up*, vol. 55. Geological Society of London Memoirs, pp. 649–664.
- Narcisi, B., Petit, J.R., Chappellaz, J., 2010a. A 70 ka record of explosive eruptions from the TALDICE ice core (Talos Dome, East Antarctic plateau). *J. Quat. Sci.* 25, 844–849.
- Narcisi, B., Petit, J.R., Delmonte, B., 2010b. Extended East Antarctic ice-core tephrostratigraphy. *Quat. Sci. Rev.* 29, 21–27.
- Narcisi, B., Petit, J.R., Delmonte, B., Basile-Doelsch, I., Maggi, V., 2005. Characteristics and sources of tephra layers in the EPICA-Dome C ice record (East Antarctica): implications for past atmospheric circulation and ice core stratigraphic correlations. *Earth Planet. Sci. Lett.* 239, 253–265.
- Narcisi, B., Petit, J.R., Delmonte, B., Batanova, V., Savarino, J., 2019. Multiple sources for tephra from AD 1259 volcanic signal in Antarctic ice cores. *Quat. Sci. Rev.* 210, 164–174.
- Narcisi, B., Petit, J.R., Delmonte, B., Scarchilli, C., Stenni, B., 2012. A 16,000-yr tephra framework for the Antarctic ice sheet: a contribution from the new Talos Dome core. *Quat. Sci. Rev.* 49, 52–63.
- Narcisi, B., Propositto, M., Frezzotti, M., 2001. Ice record of a 13<sup>th</sup> century explosive volcanic eruption in northern Victoria Land, East Antarctica. *Antarct. Sci.* 13, 174–181.
- Palais, J.M., Germani, M.S., Zielinski, G.A., 1992. Inter-hemispheric transport of volcanic ash from a 1259 AD volcanic eruption to the Greenland and Antarctic ice sheets. *Geophys. Res. Lett.* 19, 801–804.
- Palais, J.M., Kirchner, S., Delmas, R.J., 1990. Identification of some global volcanic horizons by major element analysis of fine ash in Antarctic ice. *Ann. Glaciol.* 14, 216–220.
- Palais, J.M., Kyle, P.R., Mosley-Thompson, E., Thomas, E., 1987. Correlation of a 3,200 year old tephra in ice cores from Vostok and South Pole Stations, Antarctica. *Geophys. Res. Lett.* 14, 804–807.
- Palais, J.M., Petit, J.R., Loria, C., Korotkevich, Y.S., 1989. Tephra layers in the Vostok ice core: 160,000 years of southern hemisphere volcanism. *Antarctic Journal Review* 24, 98–100.
- Pearce, J.A., Baker, P.E., Harvey, P.K., Luff, I.W., 1995. Geochemical evidence for subduction fluxes, mantle melting and fractional crystallization beneath the South Sandwich island arc. *J. Petrol.* 36, 1073–1109.
- Pearce, N.J.G., Abbott, P.M., Martin-Jones, C., 2014. Microbeam methods for the analysis of glass in fine grained tephra deposits: a SMART perspective on current and future trends. In: Austin, W.E.N., Abbott, P.M., Davies, S.M., Pearce, N.J.G., Wastegård, S. (Eds.), *Marine Tephrochronology*, vol. 398. Geological Society of London Special Publication, pp. 29–46.
- Pearce, N.J.G., Perkins, W.T., Westgate, J.A., Wade, S.C., 2011. Trace-element microanalysis by LA-ICP-MS: the quest for comprehensive chemical characterisation of single, sub-10 µm volcanic glass shards. *Quat. Int.* 246, 57–81.
- Pearce, N.J.G., Westgate, J.A., Preece, S.J., Eastwood, W.J., Perkins, W.T., 2004. Identification of Aniakchak (Alaska) tephra in Greenland ice core challenges the 1645 BC date for Minoan eruption of Santorini. *G-cubed* 5.
- Pearson, C., Sigl, M., Burke, A., Davies, S., Kurbatov, A., Severi, M., Cole-Dai, J., Innes, H., Albert, P.G., Helmick, M., 2022. Geochemical ice-core constraints on the timing and climatic impact of Aniakchak II (1628 BCE) and Thera (Minoan) volcanic eruptions. *PNAS Nexus* 1, pgac048.
- Peccerillo, A., Taylor, S.R., 1976. Geochemistry of Eocene calc-alkaline volcanic rocks from the Kastamonu area, Northern Turkey. *Contrib. Mineral. Petrol.* 58, 63–81.
- Perkins, M.E., Brown, F.H., Nash, W.P., Williams, S.K., McIntosh, W., 1998. Sequence, age and source of silicic fallout tuffs in middle to late Miocene basins of the northern Basin and Range province. *Geol. Soc. Am. Bull.* 110 (3), 344–360.
- Perkins, M.E., Nash, W.P., Brown, F.H., Fleck, R.J., 1995. Fallout tuffs of trapper creek, Idaho – a record of miocene explosive volcanism in the snake river plain volcanic province. *Geol. Soc. Am. Bull.* 107 (12), 1484–1506.
- Piva, S.B., Barker, S.J., Iverson, N.A., Winton, V.H.L., Bertler, N.A.N., Sigl, M., Wilson, C.J.N., Dunbar, N.W., Kurbatov, A.V., Carter, L., Charlton, B.L.A., Newnham, R.M., 2023. Volcanic glass from the 1.8 ka Taupo eruption (New Zealand) detected in Antarctic ice at ~230 CE. *Sci. Rep.* 13, 16720.
- Plunkett, G., Pearce, N.J.G., McConnell, J., Pilcher, J., Sigl, M., Zhao, H., 2017. Trace element analysis of Late Holocene tephras from Greenland ice cores. *Quat. Newslett.* 143, 10–20.
- Plunkett, G., Sigl, M., McConnell, J.R., Pilcher, J.R., Chellman, N.J., 2023. The significance of volcanic ash in Greenland ice cores during the Common Era. *Quat. Sci. Rev.* 301, 107936.

- Plunkett, G., Sigl, M., Pilcher, J.R., McConnell, J.R., Chellman, N., Steffensen, J.P., Büntgen, U., 2020. Smoking guns and volcanic ash: the importance of sparse tephras in Greenland ice cores. *Polar Res.* 39.
- Plunkett, G., Sigl, M., Schwaiger, H.F., Tomlinson, E.L., Toohey, M., McConnell, J.R., Pilcher, J.R., Hasegawa, T., Siebe, C., 2022. No evidence for tephra in Greenland from the historic eruption of Vesuvius in 79 CE: implications for geochronology and paleoclimatology. *Clim. Past* 18, 45–65.
- Ruth, U., Wagenbach, D., Steffensen, J.P., Bigler, M., 2003. Continuous records of microparticle concentration and size distribution in the central Greenland NGRIP ice core during the last glacial period. *J. Geophys. Res.* 108, 4098.
- Salzer, M.W., Bunn, A.G., Graham, N.E., Hughes, M.K., 2014. Five millennia of paleotemperature from tree-rings in the Great Basin, USA. *Clim. Dynam.* 42, 1517–1526.
- Severi, M., Becagli, S., Traversi, R., Udisti, R., 2015. Recovering paleo-records from antarctic ice-cores by coupling a continuous melting device and fast ion chromatography. *Anal. Chem.* 87, 11441–11447.
- Shane, P.A.R., Froggatt, P.C., 1992. Composition of widespread volcanic glass in deep-sea sediments of the Southern Pacific Ocean: an Antarctic source inferred. *Bull. Volcanol.* 54, 595–601.
- Sigl, M., Fudge, T.J., Winstrup, M., Cole-Dai, J., Ferris, D., McConnell, J.R., Taylor, K.C., Welten, K.C., Woodruff, T.E., Adolphi, F., Bisiaux, M., Brook, E.J., Buizert, C., Caffee, M.W., Dunbar, N.W., Edwards, R., Geng, L., Iverson, N., Koffman, B., Layman, L., Maselli, O.J., McGwire, K., Muscheler, R., Nishizumi, K., Pasteris, D.R., Rhodes, R.H., Sowers, T.A., 2016. The WAIS Divide deep ice core WD2014 chronology – Part 2: annual-layer counting (0–31 ka BP). *Clim. Past* 12, 769–786.
- Sigl, M., McConnell, J.R., Layman, L., Maselli, O., McGwire, K., Pasteris, D., Dahl-Jensen, D., Steffensen, J.P., Vinther, B., Edwards, R., Mulvaney, R., Kipfstuhl, S., 2013. A new bipolar ice core record of volcanism from WAIS Divide and NEEM and implications for climate forcing of the last 2000 years. *J. Geophys. Res.* 118 (3), 1151–1169.
- Sigl, M., McConnell, J.R., Toohey, M., Curran, M., Das, S.B., Edwards, R., Isaksson, E., Kawamura, K., Kipfstuhl, S., Krüger, K., Layman, L., Maselli, O.J., Motizuki, Y., Motoyama, H., Pasteris, D.R., Severi, M., 2014. Insights from Antarctica on volcanic forcing during the Common Era. *Nat. Clim. Change* 4, 693–697.
- Sigl, M., Toohey, M., McConnell, J.R., Cole-Dai, J., Severi, M., 2022. Volcanic stratospheric sulfur injections and aerosol optical depth during the Holocene (past 11,500 years) from a bipolar ice core array. *Earth Syst. Sci. Data* 14, 3167–3196.
- Sigl, M., Winstrup, M., McConnell, J.R., Welten, K.C., Plunkett, G., Ludlow, F., Büntgen, U., Caffee, M., Chellman, N., Dahl-Jensen, D., Fischer, H., Kipfstuhl, S., Kostick, C., Maselli, O.J., Mekhaldi, F., Mulvaney, R., Muscheler, R., Pasteris, D.R., Pilcher, J.R., Salzer, M., Schüpbach, S., Steffensen, J.P., Vinther, B.M., Woodruff, T.E., 2015. Timing and climate forcing of volcanic eruptions for the past 2,500 years. *Nature* 523, 543–549.
- Smellie, J.L., 1990. Graham Land and South Shetland islands – summary. In: LeMasurier, W.E., Thomson, J.W. (Eds.), *Volcanoes of the Antarctic Plate and Southern Oceans*, vol. 48. Antarctic Research Series, pp. 303–312.
- Smellie, J.L., 1999. The upper Cenozoic tephra record in the south polar region: a review. *Global Planet. Change* 21, 51–70.
- Smith, V.C., Costa, A., Aguirre-Díaz, G., Pedrazzi, D., Scifo, A., Plunkett, G., Poret, M., Tournigand, P.-Y., Miles, D., Dee, M.W., McConnell, J.R., Sunyé-Puchol, Dávila Harris, P., Sigl, M., Pilcher, J.R., Chellman, N., Gutiérrez, E., 2020. The magnitude and impact of the 431 CE tierra Blanca Joven eruption of Ilopango, El Salvador. *Proc. Natl. Acad. Sci. USA* 117, 26061–26068.
- Stokes, C.R., Abram, N.J., Bentley, M.J., Edwards, T.L., England, M.H., Foppert, A., Jamieson, S.S.R., Jones, R.S., King, M.A., Lenaerts, J.T.M., Medley, B., Miles, B.W.J., Paxman, G.J.G., Ritz, C., Van de Flierdt, T., Whitehouse, P.L., 2022. Response of the East Antarctic ice sheet to past and future climate change. *Nature* 608, 275–286.
- Tesi, T., Belt, S.T., Gariboldi, K., Muschitello, F., Smik, L., Finocchiaro, F., Giglio, F., Colizza, E., Gazzurra, G., Giordano, P., Morigli, C., Capotondi, L., Nogarotto, A., Köseoglu, D., Di Roberto, A., Gallerani, A., Langone, L., 2020. Resolving sea ice dynamics in the north-western Ross Sea during the last 2.6 ka: from seasonal to millennial timescales. *Quat. Sci. Rev.* 237, 106299.
- Toohey, M., Sigl, M., 2017. Volcanic stratospheric sulfur injections and aerosol optical depth from 500 BCE to 1900 CE. *Earth Syst. Sci. Data* 9, 809–831.
- Torricella, F., Melis, R., Malinverno, E., Fontolan, G., Bussi, M., Capotondi, L., Del Carlo, P., Di Roberto, A., Geniram, A., Kuhn, G., Khim, B.-K., Morigli, C., Scatene, B., Colizza, E., 2021. Environmental and Oceanographic conditions at the Continental margin of the central basin, Northwestern Ross Sea (Antarctica) since the last glacial Maximum. *Geosciences* 11, 155.
- Wallace, K.L., Bursik, M.I., Kuehn, S., Kurbatov, A.V., Abbott, P.M., Bonadonna, C., Cashman, K., Davies, S.M., Jensen, B., Lane, C., Plunkett, G., Smith, V.C., Tomlinson, E., Thordarsson, T., Walker, J.D., 2022. Community established best practice recommendations for tephra studies – from collection through analysis. *Sci. Data* 9, 447.